Developmental Biology 372 (2012) 249–262

Contents lists available at SciVerse ScienceDirect

Developmental Biology

journal homepage: www.elsevier.com/locate/developmentalbiology

Genetic dissection of midbrain dopamine neuron development *in vivo*

Debra Ellisor [a], Caroline Rieser [a], Bettina Voelcker [a], Jason T. Machan [b], Mark Zervas [a,*,1]

[a] Department of Molecular Biology, Cell Biology and Biochemistry, Division of Biology and Medicine, Brown University, 70 Ship St., Providence, RI 02903, USA
[b] Departments of Orthopedics and Surgery at Rhode Island Hospital and the Warren Alpert Medical School at Brown University, Providence, RI 02903, USA

ARTICLE INFO

Article history:
Received 27 October 2011
Received in revised form
10 September 2012
Accepted 23 September 2012
Available online 4 October 2012

Keywords:
Midbrain
Dopamine neurons
Wnt1
Fgf8
Engrailed
ventral tegmental area

ABSTRACT

Midbrain dopamine (MbDA) neurons are partitioned into medial and lateral cohorts that control complex functions. However, the genetic underpinnings of MbDA neuron heterogeneity are unclear. While it is known that *Wnt1*-expressing progenitors contribute to MbDA neurons, the role of *Wnt1* in MbDA neuron development *in vivo* is unresolved. We show that mice with a spontaneous point mutation in *Wnt1* have a unique phenotype characterized by the loss of medial MbDA neurons concomitant with a severe depletion of *Wnt1*-expressing progenitors and diminished LMX1a-expressing progenitors. *Wnt1* mutant embryos also have alterations in a hierarchical gene regulatory loop suggesting multiple gene involvement in the *Wnt1* mutant MbDA neuron phenotype. To investigate this possibility, we conditionally deleted *Gbx2*, *Fgf8*, and *En1/2* after their early role in patterning and asked whether these genetic manipulations phenocopied the depletion of MbDA neurons in *Wnt1* mutants. The conditional deletion of *Gbx2* did not result in re-positioning or distribution of MbDA neurons. The temporal deletion of *Fgf8* did not result in the loss of either LMX1a-expressing progenitors nor the initial population of differentiated MbDA neurons, but did result in a complete loss of MbDA neurons at later stages. The temporal deletion and species specific manipulation of *En1/2* demonstrated a continued and species specific role of Engrailed genes in MbDA neuron development. Notably, our conditional deletion experiments revealed phenotypes dissimilar to *Wnt1* mutants indicating the unique role of *Wnt1* in MbDA neuron development. By placing *Wnt1*, *Fgf8*, and *En1/2* in the context of their temporal requirement for MbDA neuron development, we further deciphered the developmental program underpinning MbDA neuron progenitors.

Introduction

Midbrain dopamine (MbDA) neurons mediate a diverse array of complex behaviors including cognition and motor control. MbDA neurons are located in the ventral Mb (v. Mb) and are broadly delineated as a medial group (the ventral tegmental area, VTA) and two bi-lateral cohorts (the substantia nigra *pars compacta*, SNc). In addition to their anatomical differences, MbDA neurons are also molecularly, biochemically, and physiologically distinct (Mendez et al., 2005; Parent, 1996; Thompson et al., 2005; Grimm et al., 2004). Clinically, the distinction between VTA and SNc is important because the aberrant function of VTA MbDA neurons and the loss of SNc MbDA neurons are central features of schizophrenia and Parkinson's disease, respectively (Fallon et al., 2003; Parent, 1996). However, little is known about the developmental genetics underpinning the partitioning of MbDA neurons into medial and lateral MbDA neuron cohorts.

The Mb is derived from the mesencephalon (mes), which is an embryonic compartment that is patterned through the interactions of numerous transcription factors and cell signaling molecules, which include *Otx2*, *Gbx2*, *En1/2*, *Fgf8*, *Shh*, and *Wnt1* (reviewed in Zervas et al., 2005). Notably these genes also play varying roles in the induction, positioning, differentiation, and survival of v. mes progenitors (reviewed in Goridis and Rohrer, 2002; Prakash and Wurst, 2006; Zervas et al., 2005). We previously marked and tracked MbDA progenitors using Genetic Inducible Fate Mapping (GIFM), which uncovered that MbDA neurons are derived from the *Wnt1* lineage originating in the v. mes (Zervas et al., 2004; Brown et al., 2011). Gain-of-function studies *in vitro* suggest that *Wnt1* has a role in MbDA neuron induction and differentiation (Castelo-Branco et al., 2003; Prakash and Wurst, 2006). Recently, chromatin immunoprecipitation-qPCR reveals that *Wnt1*directly regulates a MbDA neuron determinant, *Lmx1a*, through β-catenin signaling (Chung et al., 2009). However, whether *Wnt1* is required for MbDA neuron development *in vivo* has been elusive because

* Correspondence to: Laboratory of Developmental Neurobiology, Genetics and Neurological Disease, Department of Molecular Biology, Cell Biology and Biochemistry, Division of Biology and Medicine, Box G-E436, Brown University, Providence, RI 02903, USA. Fax: +1 401 863 9653.
E-mail address: Mark_Zervas@brown.edu (M. Zervas).
URL: http://research.brown.edu/myresearch/Mark_Zervas (M. Zervas).
[1] Courier delivery: Laboratories for Molecular Medicine, 70 Ship Street, Rm. 436, Providence, RI 02903, USA.

0012-1606/$ - see front matter © 2012 Elsevier Inc. All rights reserved.
http://dx.doi.org/10.1016/j.ydbio.2012.09.019

mice homozygous for a targeted allele of *Wnt1* die perinatally and have a patterning defect concomitant with a complete deletion of the Mb and cerebellum (Cb) (McMahon and Bradley, 1990; Thomas et al., 1991; McMahon et al., 1992).

We utilized mice that have a point mutation in *Wnt1* (*Wnt1*$^{SW/SW}$) and a large deletion of the Mb and Cb, but live to adulthood (Lane, 1967; Sidman, 1968; Thomas et al., 1991). The v. Mb in *Wnt1*$^{SW/SW}$ mice has not been extensively studied. Here, we use *Wnt1*$^{SW/SW}$ mice to investigate the *in vivo* requirement of *Wnt1* for the establishment of MbDA neurons during embryogenesis. The initial patterning of the mes is intact in mutant mice although *Wnt1*-expressing MbDA neuron progenitors are significantly depleted prior to differentiation, which correlates with the loss of VTA MbDA neurons in adults. Because *Wnt1* is involved in a genetic hierarchical loop that is compromised in *Wnt1*$^{SW/SW}$ mutants, we used conditional gene inactivation to assess how the deletion of genes affected in mutant embryos impacted MbDA neuron development. The conditional deletion of *Fgf8*, *Gbx2*, or *En1*/*En2* after their well-defined roles in patterning did not phenocopy the *Wnt1*$^{SW/SW}$ MbDA neuron abnormalities. Our findings show that genes required for patterning the mes have distinct temporal roles in MbDA neuron development *in vivo*. Finally, *Wnt1*$^{SW/SW}$ mice are poised to be a value research tool to study how the absence of VTA MbDA neurons affects brain function and behavior.

Materials and methods

Transgenic, reporter, and mutant mice

Wnt1$^{SW/SW}$ mice (stock ♯ 000243) were obtained from The Jackson Laboratory on a mixed C57Bl/6 background. We outbred the mice onto a Swiss Webster background to improve the general litter sizes and the *Wnt1*$^{SW/SW}$ phenotype was indistinguishable between both strains. Our analysis was performed on the latter background, which we have maintained for the last eight years. *En1*^{Cre} mice (Kimmel et al., 2000) were used to mediate the conditional knockout (cko) of the following floxed alleles: *Gbx2*^{lox} (Li et al., 2002), *En1*^{lox} (Sgaier et al., 2007) and *Fgf8*^{lox} (Chi et al., 2003). In addition, we used *Rosa26*^{CreERT2};*En1*$^{lox/-}$;*En2*$^{GFPlox/-}$ mice (Cheng et al., 2010) and *En1*^{Den} mice (Hanks et al., 1998; Sgaier et al., 2007). *Fgf8*^{lox} mice were generously provided by G. Martin and all other lines were generously provided by A. Joyner. Mice were maintained and sacrificed according to the protocols approved by the Institutional Animal Care and Use Committee (IACUC) at Brown University (IACUC ♯0909081). *Wnt1-Venus* transgenic mice were generated by placing a *GFP* variant, *Venus* that encodes *YFP*, under the control of Wnt1 regulatory elements (See Brown et al., 2011 for details). This was done by replacing the *CreER*^{T} cassette with *YFP* in the vector used to generate *Wnt1-CreER*^{T} transgenic mice (Zervas et al., 2004). Embryos were staged in reference to embryonic day (E)0.5 being prior to noon of the day of the appearance of a vaginal plug.

Genotyping of Wnt1$^{+/+}$*;Wnt1-Venus, or Wnt1*$^{SW/+}$*;Wnt1-Venus, and Wnt1*$^{SW/SW}$*;Wnt1-Venus embryos for Fluorescent Activated Cell Sorting (FACS)*

A tail biopsy was obtained from each embryo prior to pooling to confirm the genotype of samples used for FACS. Because the *Wnt1-Venus* transgene has *YFP* placed between the untranslated region (UTR) and translated region of exon 1 and the transgene also contains the sequence for *Wnt1* (See Brown et al., 2011 for details) essentially all homozygotes appear as heterozygotes when genotyping using a routine PCR strategy. To overcome this issue we designed a three-phase PCR/restriction digest strategy to unambiguously identify *Wnt1*$^{SW/SW}$ embryos. First, we used the primers p*Wnt1.F3* (*ACAGCAACCACAGTCGTC*) and *Wnt1*ex2_3rev (*CTGAGATAGGGACATTCGG*), which anneal to the UTR in exon 1 and in the intronic region upstream of exon 3, respectively. These primers amplify a 2 kilobase (kb) amplicon corresponding to endogenous *Wnt1* alleles or a 3 kb amplicon corresponding to the *Wnt1-Venus* transgene (due to the YFP insert). The two amplicons were separated on a 1.4% agarose gel and the 2 kb band was gel extracted using the Qiaquick gel extraction kit. Subsequently, a second PCR reaction was done using the *Wnt1.sense* (*AGGAACCTCTTTGCCCTCAACC*) and *Wnt1.anti-sense* (*AAGTTCATCTGCACCACCG*) primers followed by BSLI restriction digest to discern between the *Wnt1*$^{+/+}$, *Wnt1*$^{SW/+}$, and *Wnt1*$^{SW/SW}$ alleles. The point mutation in the *Wnt1*^{SW} allele creates a distinct BSLI digest pattern, which always matched the embryos originally identified by phenotyping as described above.

Tissue preparation, in situ hybridization, and immunofluorescent immunocytochemistry (IF-ICC)

All embryos and adult tissues were prepared as previously described (Ellisor et al., 2009; Brown et al., 2011). Briefly, embryos were fixed in 4% paraformaldehyde (PFA) overnight (o/n) at 4 °C. Embryos were processed for whole mount *in situ* hybridization or were embedded in OCT as previously described (Ellisor et al., 2009). Cryoprotected tissue was frozen using 2-methyl-butane/acetone (http://home.primus.com.au/royellis/fr.htm) and blocks were stored at −20 °C. Embryonic material was cryosectioned at 10–12 μm and collected directly onto slides and stored at −20 °C until used. For adult tissue, mice were deeply anesthetized with beuthanasia-D. Once mice were unresponsive to deep hind paw pinch, the mice were flushed with saline and fixed with PFA by intracardiac perfusion as previously described (Brown et al., 2009). Brains were immersion fixed overnight (o/n) and stored in PBS. Adult sections (40 μm) were obtained with a Leica VT1000S vibratome and stored free floating at stored at 4 °C until used. Protocol details are available at the Zervas Lab web page (http://research.brown.edu/myresearch/Mark_Zervas). Whole mount RNA *in situ* hybridization was performed on E8.5, E9.5, and E10.5 embryos using antisense digoxigenin labeled RNA probes as previously described (Zervas et al., 2004; Ellisor et al., 2009). Sections for IF-ICC were fixed for five minutes, washed in PBT five times, and blocked in 10% donkey serum/PBT for two hours at room temperature. Sections were incubated with primary antibody (Ab) in 10% donkey serum o/n at 4 °C. The next day sections were washed in PBT five times. Subsequently, sections were incubated with secondary Abs in 1% donkey serum/PBT for two hours, washed in PBT five times, and counterstained with Hoechst nuclear dye (Molecular Probes) for one minute. Images were collected and processed using Open Lab, Magnafire, or Volocity 5.2 (Improvision) software and Adobe Photoshop or Illustrator CS2.

Primary antibodies: Dopaminergic, serotonergic, and cholinergic neurons were detected with anti-tyrosine hydroxylase (TH, Chemicon; 1:500), anti-5-hydroxytryptamine (5-HT, Jackson ImmunoResearch; 1:500), and anti-choline acetyl transferase (ChAT, Chemicon; 1:100), respectively. Calbindin (CALB) and g-protein inward rectifying potassium (K) channel 2 (GIRK2) were detected with anti-CALB (Swant; 1:1000) or anti-Girk2 (Alomone labs; 1:80), respectively. LMX1a Ab was generously provided by Michael German (UCSF, 1:1000). Secondary antibodies (Molecular Probes; all used at 1:500): donkey anti-mouse IgG-AMCA, donkey anti-mouse IgG-Alexa350, donkey anti-mouse IgG-Alexa555, donkey anti-mouse IgG-Alexa488, donkey anti-rabbit IgG-Alexa488, donkey anti-goat IgG-Alexa555.

Fluorescent activated cell sorting (FACS) and quantification of embryonic phenotype

The v. mes of *Wnt1*$^{+/+}$;*Wnt1-Venus*, *Wnt1*$^{SW/+}$;*Wnt1-Venus*, or *Wnt1*$^{SW/SW}$;*Wnt1-Venus* embryos was microdissected as previously described (Brown et al., 2009). Briefly, we removed embryos and used a stereofluorescent microscope to observe YFP-expressing domains. We isolated the v. mes by cutting along the rostral-caudal axis directly adjacent to the dorsal midline, which yielded a butterfly shaped tissue with the *v*. mes at the center. The small domain of YFP-expressing cells was carefully dissected away from the posterior mes "ring" and dorsal tissue (Brown et al., 2009). The v. mes of putative *Wnt1*$^{+/+}$;*Wnt1-Venus* and *Wnt1*$^{SW/+}$;*Wnt1-Venus* embryos, initially identified by an intact mes and rhombomere 1 (r1), were pooled prior to FACS (Fig. 3A). We also isolated the v. mes from morphologically distinct *Wnt1*$^{SW/SW}$;*Wnt1-Venus* mutant embryos (identified by a truncated dorsal mes/r1 (Fig. 3B); embryos were genotyped as described below. For FACS, the v. mes issue was trypsinized using TryplE Express (Gibco) and DNase (Roche) at 1:1000 for eight minutes at 37 °C. Subsequently, 10% FBS/PBS was added to stop the reaction. Samples were then mechanically dissociated using a 20-gauge needle and 1cc syringe to generate a single cell suspension. Cells were stored on ice until sorting with a FACSAria flow cytometer (BD) and analyzed using Diva software (BD) at Brown University's Flow Cytometry and Sorting Facility. Population gates were established by setting threshold values based on wildtype littermate control samples and YFP-negative internal control samples obtained from the prosencephalon. YFP-positive cells from the microdissected tissue samples were counted and analyzed for forward and side scatter. FACS isolated cells were collected into an eppendorf tube and an aliquot plated and analyzed by fluorescent microscopy to validate the enrichment of YFP+ cells. A subset of sagittal sections encompassing the midline and off-midline planes from E10.5 embryos (Brown et al., 2011) were manually counted for YFP+ progenitors and either LMX1a or OTX2- expression. Multiple embryo counts were pooled and the average ± standard deviation was plotted in Numbers. Notably, the extent of calculated cellular loss was similar between the whole population counts (FACS) and subsampled embryos (Marker analysis). Cell counts from FACS and sections were compared for significance using 2-tailed Students *T*-test.

Quantification and statistical analysis of adult phenotype

Wnt1$^{SW/SW}$ and control (*Wnt1*$^{sw/+}$ or *Wnt1*$^{+/+}$) mice ($n=3$, each genotype) were perfused, embedded and sectioned on the vibratome as described above. We collected sections encompassing the entire MbDA neuron population. Three sections were chosen for analysis: a ventral plane (−4.56 mm), an intermediate plane (−4.12 mm) and a dorsal plane (−3.76 mm) using bregma as a reference as previously described (Brown et al., 2011). Sections were processed and immunolabeled for TH, calbindin, and GIRK2 as described above. We acquired 20× z-series images through the full thickness of each section, collecting 1 μm thick optical planes using Volocity 5.2. All images were taken using the same red, green and blue filter settings to ensure consistency. Three random, non-overlapping counting frames for each section were acquired from the SNc on each side of the brain and from the VTA for a total of nine counting frames acquired per section. The red channel corresponding to either calbindin or GIRK2 was cloaked and a single optical sectioning plane was chosen for counting. TH+ neurons (distinguished as single cells) were counted by an observer blinded to the genotype of the mice, marked using the point tool, and recorded. The red channel was subsequently uncloaked and double positive cells were quantitated in a similar manner and recorded. This resulted in six counting frames of TH+ and double positive neurons in the SNc and three counting frames of TH+ and double positive neurons in the VTA for each section at each plane for each animal. The average number of TH+ and double positive neurons was calculated for the VTA and SNc from animals of each genotype in each horizontal sectioning plane: dorsal, intermediate or ventral. Results from animals with the same genotype were pooled.

Generalized linear models (Nelder and Wedderburn, 1972) were used to compare across genotypes for the following items: 1. Total TH cell counts (Poisson). 2. Counts of TH cells co-stained with CALB or GIRK (Poisson). 3. The proportion of TH cells co-stained with CALB or GIRK (binomial). A cell means model approach was taken owing to the small sample size, allowing fewer parameters to be estimated by eliminating omnibus tests for interactions. Genotypes were compared as effect slices at each location within each structure (VTA and SNc). Sandwich estimation was used to adjust for any model misspecification (Huber, 1967; White, 1980; Hinkley, 1977), adjusted for the small sample size based on the degrees of freedom (Hinkley, 1977; Fay and Graubard, 2001; Kauermann and Carroll, 2001) that were manually set to 4 for all slice comparisons between genotypes ($n=3$ for each genotype in each comparison, $df=(3-1)+(3-1)$). There were no double immunolabeled GIR2K^{+}/TH^{+} neurons observed in the ventral VTA of any of the mutant GIRK2-stained slices. This constituted a division by zero within the model and invalidated the estimate. Therefore, the p-values generated in the comparison between mutant and wildtype mice GIRK2 counts in the ventral VTA and proportions are not used.

Results

To facilitate our understanding of the role of *Wnt1* in MbDA neuron development, we utilized mice with the spontaneous *Swaying* mutation (allele designated as *Wnt1*^{SW}) (Lane, 1967). The *Wnt1*^{SW} allele has a point mutation (*G*^{565}) in the third exon of *Wnt1* resulting in a premature TGA stop codon 30 base pairs downstream from the point mutation (Thomas et al., 1991). *Wnt1*$^{SW/SW}$ homozygotes were detected at a frequency of 6% ($n=366$ adults) from *Wnt1*$^{SW/+}$ intercrosses instead of the predicted 25%. Notably, all homozygotes had a prominent ataxic gait and a striking bi-directional rotation behavior (See Movies 1 and 2). The survival of *Wnt1*$^{SW/SW}$ mice provided an advantage over *Wnt1* null mice, which do not survive postnatally (McMahon and Bradley, 1990). Therefore, we used *Wnt1*$^{SW/SW}$ survivors to assess the long-term impact of perturbing *Wnt1* on MbDA neuron populations.

Supplementary material related to this article can be found online at doi:10.1016/j.ydbio.2012.09.019.

Biased loss of VTA MbDA neurons in adult Wnt1$^{SW/SW}$ *mice*

We initially assessed the MbDA neurons of wildtype and *Wnt1*$^{SW/SW}$ adult mice with TH immunolabeling. Compared to wildtype littermates (Fig. 1A and B), *Wnt1*$^{SW/SW}$ mice (Fig. 1H and I) ($n=5$ each genotype) had a complete loss of the medially positioned MbDA neurons, presumptively the VTA. *Wnt1*$^{SW/SW}$ mutants also had a reduction of MbDA neurons located adjacent to the medial population in the presumptive SNc (Fig. 1C and J, bracket), although this was substantially less pronounced than the loss of medial MbDA neurons (Fig. 1B and I). The evaluation of ChAT immunolabeling, which delineates cholinergic neurons (Manger et al., 2002; Woolf, 1991) revealed cholinergic neurons interspersed in the rostral SNc of adult *Wnt1*$^{SW/SW}$ mice (insets in Fig. 1C and J). However, we did not observe detectable changes in cholinergic axons that course through the v. Mb (Fig. 1B and I).

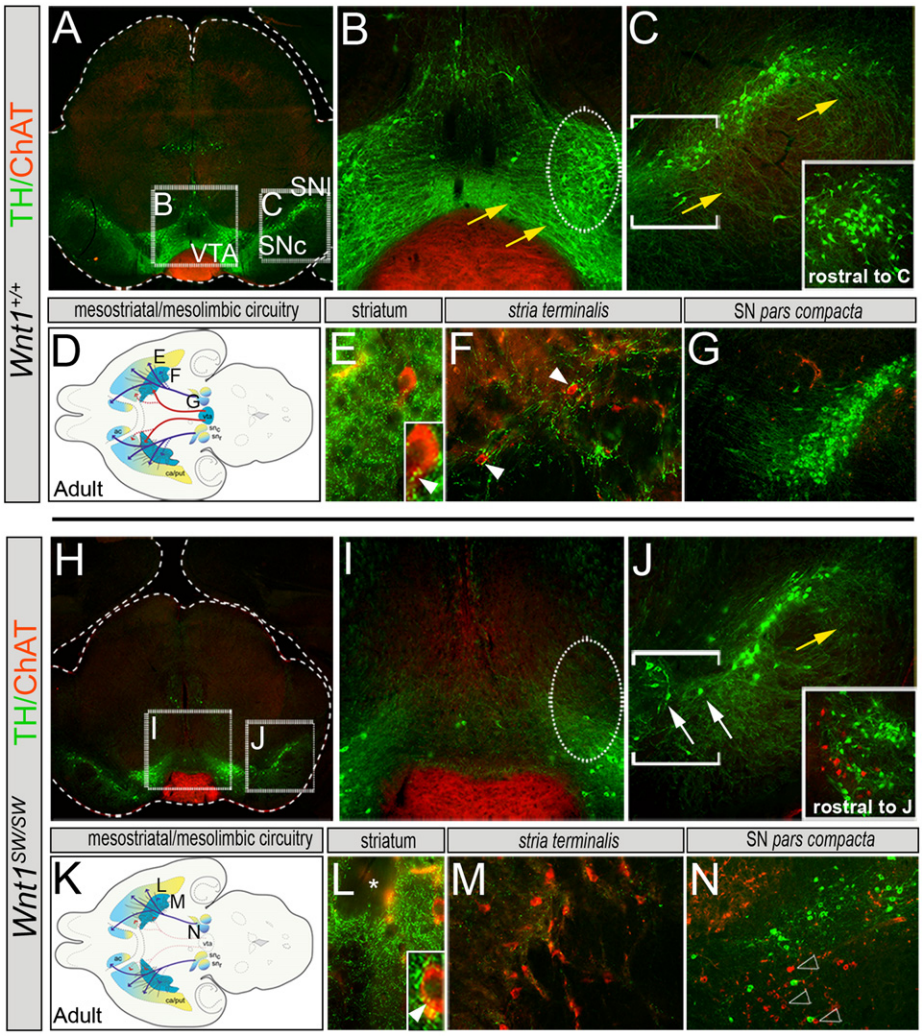

Fig. 1. Loss of MbDA neurons in adult *Wnt1*$^{SW/SW}$ mice. (A–C) Coronal sections of adult wildtype mouse immunolabeled with antibodies against TH (green) and ChAT (red). (A) Medial and lateral MbDA neurons and cholinergic axons in the v. Mb. (B, C) Medial (B) and lateral (C) MbDA neuron somata (oval marquee) and dopaminergic axons (yellow arrows). Inset in C shows region just rostral to (C); bracket shows medial aspect of SNc. (D) Illustration of horizontal section showing medial and lateral MbDA neurons and their projections (red and blue arrows, respectively; dashed lines show minor contributing projections). (E) TH+ projections innervated the striatum and were closely opposed to cholinergic neurons (ChAT+, red). Inset in (E) shows high magnification of dopamine axonal terminals and white arrowhead indicates punctae opposed to Chat+ neuron. (F) TH+ projections innervated Chat+ neurons in the stria terminalis. (G) Lateral MbDA neurons of the SNc. (H,I) Coronal section of adult *Wnt1*$^{SW/SW}$ mouse showing the depletion of medial MbDA neurons; cholinergic projections were unaffected. (J) Diminished putative SNc (J; arrows point to a few remaining medial aspect of SNc). The inset shows region rostral to J′ and corresponds to inset in (C); note the presence of cholinergic neurons interspersed with SNc MbDA neurons. (K) Schematic of MbDA neuron circuitry in *Wnt1*$^{SW/SW}$ mouse. (L) Dopaminergic axons of *Wnt1*$^{SW/SW}$ mice innervated the striatum. The asterisk indicates a patch region of the striatum; Inset in (L) shows high magnification of dopamine axons adjacent to ChAT+ neuron (red); white arrowhead indicates punctae. (M) The stria terminalis of *Wnt1*$^{SW/SW}$ mice was intact and replete with cholinergic neurons, but was not innervated by MbDA axons. (N) *Wnt1*$^{SW/SW}$ mice had lateral MbDA neurons as well as ectopic cholinergic neurons (N, arrowheads indicate ectopic ChAT+ neurons). (For interpretation of the references to color in this figure legend, the reader is referred to the web version of this article.)

A well-characterized feature of MbDA neurons is that they have TH+ axonal projections that functionally link anatomically distinct regions (Fallon et al., 2003; Parent, 1996). MbDA neurons of the VTA innervate prefrontal cortex, ventral striatum, and the bed nucleus of the *stria terminalis* (BNST), which is the gateway to the striatum. MbDA neurons establish synapses on cholinergic neurons in the later two structures (Fig. 1D–F) (Berendse et al., 1992; Chang, 1988; Gaykema and Zaborszky, 1996; Hasue and Shammah-Lagnado, 2002; Kubota et al., 1987). In contrast, axons of SNc MbDA neurons (Fig. 1G) predominantly project to dorsal striatum (Fig. 1E) (Parent, 1996; Paxinos, 2004), but also have a minor contribution to the BNST (Gaykema and Zaborszky, 1996). Given the profound loss of MbDA neurons we observed in *Wnt1*$^{SW/SW}$ mice and the reciprocal BNST-to-VTA circuit typically observed in controls (Georges and Aston-Jones, 2002; Hasue and Shammah-Lagnado, 2002), we assessed dopaminergic target sites in *Wnt1*$^{SW/SW}$ mutants (Fig. 1K–N). MbDA innervation of the BNST was nearly absent although cholinergic neurons endogenous to this region were present (Fig. 1M; $n=3$). Interestingly, axons from MbDA neurons of the remaining SNc (Fig. 1N), which were presumably responsible for the innervation of the striatum (Fig. 1L), did not get re-routed into the BNST even though cholinergic neurons persisted in this domain (Fig. 1M). These data suggest that *Wnt1* is preferentially required for the development of VTA MbDA neurons. However, the loss of VTA MbDA neurons did not result in selective loss of target sites or compensatory re-routing of SNc axons into VTA targets devoid of their endogenous innervation. The loss of VTA is also apparent in horizontal sections (Supplemental Fig. 1A and C).

We quantified VTA and SNc MbDA neurons in *Wnt1*$^{SW/SW}$ adults (Fig. 2A) using an unbiased stereology approach (Brown et al., 2011) and double immunocytochemistry with antibodies that recognize TH+/CALB+ (VTA) neurons or TH+/GIRK2+ (SNc) neurons, consistent with previous reports (Mendez et al., 2005;

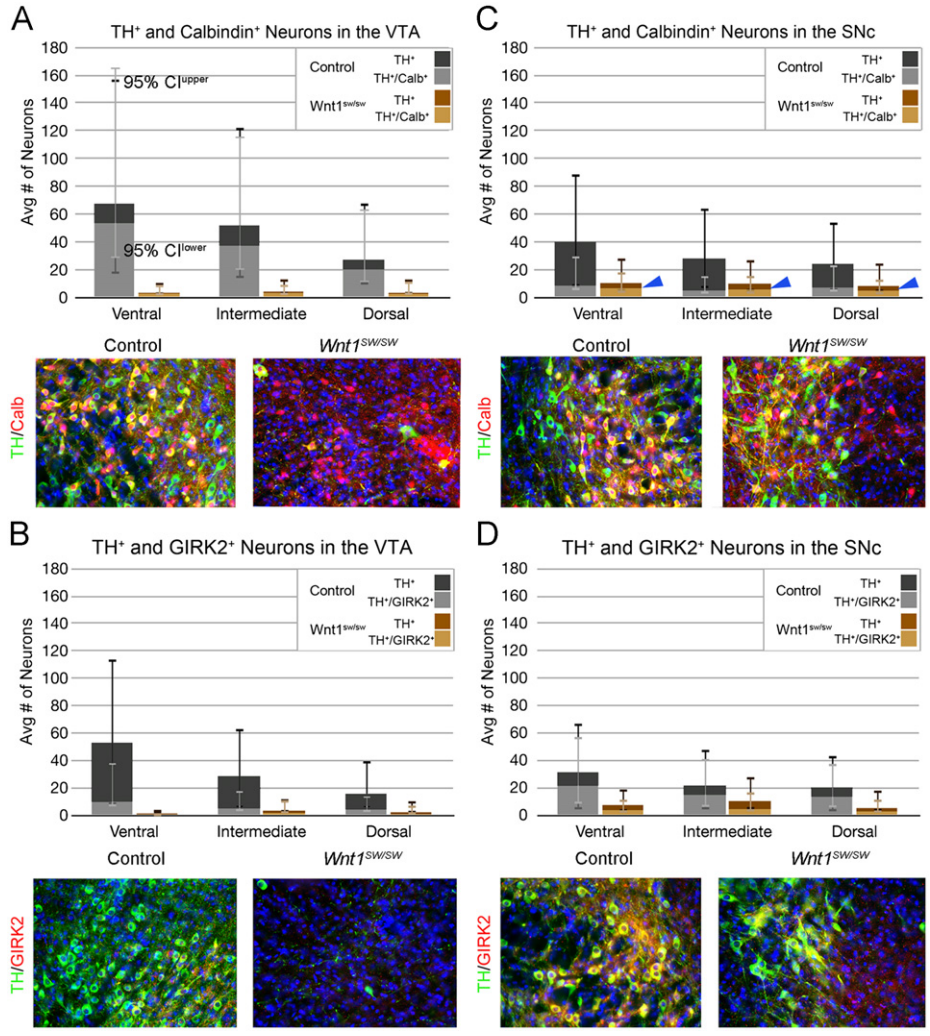

Fig. 2. Quantification of cells in control and mutant mice reveals significant differences in the average number of TH+ and double positive neurons in the VTA and SNc. The average number of TH+ neurons and the 95% confidence intervals (CI) of counts from the VTA (A, B) and SNc (C, D) of control (dark grey shaded bars) and mutant mice (dark brown bars) in ventral, intermediate and dorsal planes. (A) The average number of TH+/Calb+ neurons in the VTA of mutant mice (light brown bars) was significantly lower than that of control mice (light grey bars) in all planes quantified. Calb+ neurons in the VTA indicated that the medial domain was not devoid of cells. (B) There were no double immunolabeled $TH^+/GIR2K^+$ neurons observed in the ventral VTA of any of the mutant GIRK2-stained slices consistent with the loss of VTA. (C) Although TH+ neurons were diminished in SNc, the average number of $TH^+/Calb^+$ neurons in the SNc was not significantly different between controls (light grey bars) and mutants (light brown bars) at any of the three horizontal planes. The blue arrowheads points to the average of $TH^+/Calb^+$ neurons. (D) The average number of $TH^+/GIRK2^+$ neurons in the SNc of mutant mice was significantly lower than that of control mice in all planes quantified. Images in A, C display TH^+ (green), $Calb^+$ (red) and $TH^+/Calb^+$ (yellow) cells while images in B, D display TH^+ (green), $GIRK2^+$ (red) and $TH^+/GIRK2^+$ (yellow) cells. Gray shading of bars indicates data from control animals with dark gray bars corresponding to average TH^+ cell counts and nested light gray bars corresponding to average double positive cell counts. Brown shading indicates data from mutant animals with dark brown bars corresponding to average TH^+ cell counts and nested lighter brown bars corresponding to average double positive cell counts. (For interpretation of the references to color in this figure legend, the reader is referred to the web version of this article.)

Parent, 1996; Paxinos, 2004; Thompson et al., 2005). The average number of TH+ neurons in the VTA (Fig. 2A and B) and SNc (Fig. 2C and D) of control (dark grey bars) and mutant mice (dark brown bars) was significantly different in ventral, intermediate and dorsal planes, with mutants having fewer TH+ neurons than controls (See also Supplemental Tables 1 and 2). Comparing the loss of TH+ neurons in the VTA between controls and mutants ($P<0.0001$) and the loss of TH+ neurons in the SNc ($p=0.0001$) revealed that the loss of TH+ neurons in the VTA was significantly greater, proportionally, than the loss of TH+ neurons in the SNc ($p=0.0038$) (See for example Fig. 1 and Supplemental Fig. 1). Also graphed in Fig. 2 are the counts and 95% confidence intervals of TH+/marker+ neurons in controls (light grey bars) and mutants (light brown bars). The average number of TH+/Calb+ neurons in the VTA of mutant mice was significantly lower than that of control mice in all planes quantified (Fig. 1A, Supplemental Tables 1 and 2). There were Calb+/hoechst+ neurons in the medial domain positioned between the bilateral SNc indicating that the medial domain was not devoid of cells (Fig. 2A, inset). There were very few GIRK2+ neurons in the VTA, which were located at the margin of the VTA. Regardless, there were no double immunolabeled $TH^+/GIR2K^+$ neurons observed in the ventral VTA of any of the mutant GIRK2-stained slices. (Fig. 1B, Supplemental Tables 1 and 2). Therefore, the remaining medial tissue did not have TH+ neurons with lateral characteristics suggesting that the SNc was not displaced and that mutant VTA MbDA neurons did not change to a lateral fate. Interestingly, the average number of TH+/Calb+ neurons in the SNc was not significantly different between controls and mutants at any of the three horizontal planes (Fig. 1C, blue arrowheads; Supplemental Tables 1 and 2). These likely correspond to dorsal tier MbDA neurons (Gerfen et al., 1987). The average number of TH+/GIRK2+ neurons in the SNc of mutant mice was significantly lower than that of control mice in all planes quantified (Fig. 1D, Supplemental Tables 1 and 2). These findings indicate that

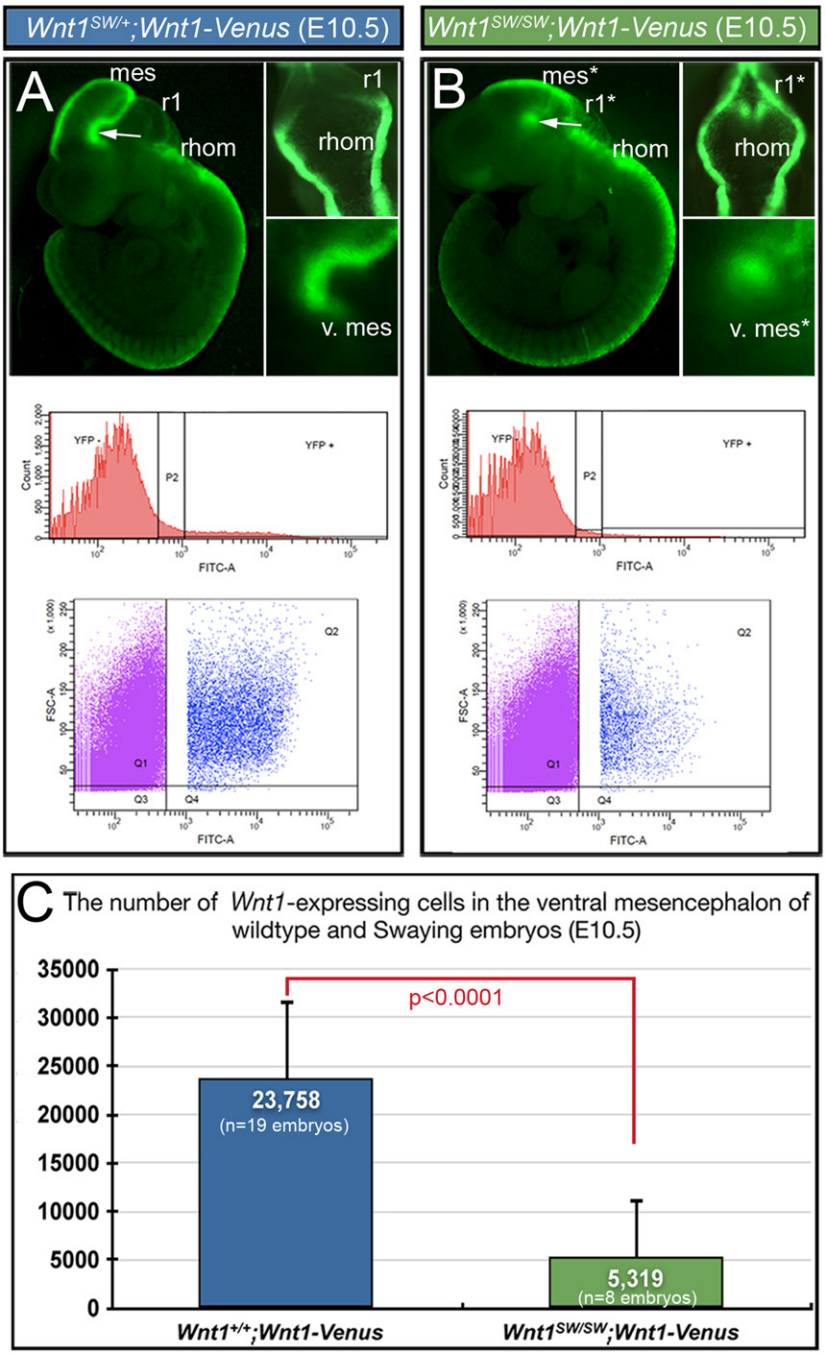

Fig. 3. Quantitative reduction in *Wnt1*-expressing progenitors in *Wnt1*$^{SW/SW}$ embryos. (A) Wholemount fluorescence in *Wnt1-Venus* transgenic embryos showing mes, r1, and hindbrain (rhombencephalon, rhom). The rhom is shown in dorsal view in top inset and the v. mes is indicated by the arrow and magnified in the lower inset. The lower panels show FACS data for a representative E10.5 *Wnt1-Venus* v. mes. (B) Wholemount fluorescence in *Wnt1*$^{SW/SW}$;*Wnt1-Venus* embryo. The v. mes progenitors were depleted compared to controls. Lower panels showing corresponding FACS analysis. Asterisks indicate domains with altered morphology. (C) Graph depicting the average number of *Wnt1*-expressing (YFP positive) cell counts obtained during FACS from the v. mes from wildtype and mutant embryos. Standard deviation and significance are shown.

the SNc loss is primarily due to decreased GIRK2+/TH+ MbDA neurons and that Calb+/TH+ MbDA neurons in SNc are refractory to *Wnt1* perturbation.

Wnt1$^{SW/SW}$ *mice have aberrant mixing of dopamine and serotonin neurons, but do not undergo degeneration*

It was previously suggested by that *Wnt1*$^{SW/SW}$ embryos have a disruption in the lineage boundary (Bally-Cuif et al., 1995). We performed triple immunolabeling with TH, ChAT and 5-HT to determine whether the general Mb/aHb cytoarchitecture was preserved in the mutants. In controls, TH+ MbDA neurons were positioned adjacent to cholinergic axons of the interpenduncular nucleus (IPn) (Supplemental Fig. 1A). In addition, controls had clearly identified 5-HT+ serotonin neurons of the dorsal Raphe nucleus (dRN), TH+ noradrenergic neurons in the locus coeruleus (LC), and cholinergic neurons of the lateral dorsal tegmental nucleus (LDTg), which were adjacent to the LC in wildtype mice (Supplemental Fig. 1B). TH+ MbDA neurons in the dorsal VTA and 5HT+ neurons of the dRN in wildtype mice did not intermingle

consistent with their segregation during development (Supplemental Fig. 1B) (Zervas et al., 2004). In contrast, *Wnt1*$^{SW/SW}$ mice had a depletion of VTA overall and had TH+ neurons interspersed amongst 5HT+ neurons of the medial RN (mRN) (Supplemental Fig. 1C, yellow arrowheads). Despite these observations, *Wnt1*$^{SW/SW}$ mutant mice did have an appropriate allocation of serotonergic, cholinergic, and noradrenergic neurons that were distributed in anatomically appropriate arrangements in the anterior Hb (Supplemental Fig. 1B and D).

We then asked whether MbDA neurons were depleted at birth or whether they were established properly, but subsequently degenerated. Therefore, we assessed mice at postnatal day (P)0 when MbDA neurons begin to appear as highly organized clusters of the VTA and SNc based on their relative position to each other and their final distribution in the adult (Paxinos, 2004) (Supplemental Fig. 2). In contrast to control littermates, *Wnt1*$^{SW/SW}$ mice ($n=3$) at P0 displayed a depletion of VTA MbDA neurons with the remaining TH positive neurons in this domain appearing as disorganized loose clusters (Supplemental Fig. 2A, B, D and E). TH+ MbDA neurons consistent with the SNc were detected, albeit diminished, in the ventral most MbDA neuron domain (Supplemental Fig. 2D and E). *Wnt1*$^{SW/SW}$ pups with a depletion of MbDA neurons had serotonergic neurons in the aHb nuclei (Supplemental Fig. 2C and F). These findings indicated that VTA MbDA neurons were depleted at birth and that the adult phenotype was not the result of later degeneration of MbDA neurons. We assayed *Wnt1*$^{SW/SW}$ mutant embryos at E11.5 when the initial wave of postmitotic TH+ neurons is typically observed *in vivo*. In wild-type embryos, MbDA neurons in the v. mes were clearly separated from serotonin neurons of v. r1 (Supplemental Fig. 3A) consistent with lineage mapping studies (Zervas et al., 2004) and their relative positions in the adult. In contrast, loose clusters of ectopic TH+ neurons were aberrantly interspersed within the adjacent 5HT+ serotonergic neurons in v. mes r1 of *Wnt1*$^{SW/SW}$ mutant embryos (Supplemental Fig. 3B), which indicates that the adult phenotype of interspersed dopamine and serotonin neurons had occurred prior to birth.

Wnt1$^{SW/SW}$ *embryos are depleted of MbDA neuron progenitors*

We next addressed whether the loss of MbDA neurons in *Wnt1*$^{SW/SW}$ mutants resulted from the loss of *Wnt1*-expressing MbDA neuron progenitors. To address this question, we bred *Wnt1-Venus* transgenic mice to *Wnt1*$^{SW/SW}$ mutants and microdissected the v. mes as previously described (Brown et al., 2009). We previously showed that *Wnt1*(GFP) from the *Wnt1-Venus* line recapitulates the temporal and spatial distribution of *Wnt1* transcripts in whole mount embryos and in section analysis (Brown et al., 2011; Hagan and Zervas, 2012). Fluorescent activated cell sorting (FACS) of YFP+ cells isolated from the v. mes of E10.5 control embryos (Fig. 3A; $n=19$) yielded an average of 23,758 ± 8220 *Wnt1*-expressing cells compared to *Wnt1*$^{SW/SW}$;*Wnt1-Venus* embryos (Fig. 3B; $n=8$) that had only on average 5319 ± 6043 *Wnt1*-expressing cells. Thus, *Wnt1*$^{SW/SW}$ mutant embryos had a significant 77.6% reduction ($P<0.0001$) of *Wnt1*-expressing cells compared to controls (Fig. 3C). Collectively, these findings indicated that *Wnt1*-expressing MbDA neuron progenitors in the v. mes were depleted, and the surviving MbDA neuron progenitors likely gave rise to the remaining MbDA neurons in adult *Wnt1*$^{SW/SW}$ mutants.

We then analyzed the molecular identity of *Wnt1*(GFP)+ progenitors in midgestation embryos (Fig. 4 and Supplemental Fig. 4 $n \geq 3$ each genotype), when *Wnt1*-expressing MbDA neuron progenitors are being specified and acquire their molecular identity (Brown et al., 2011; Hayes et al., 2011). First, we

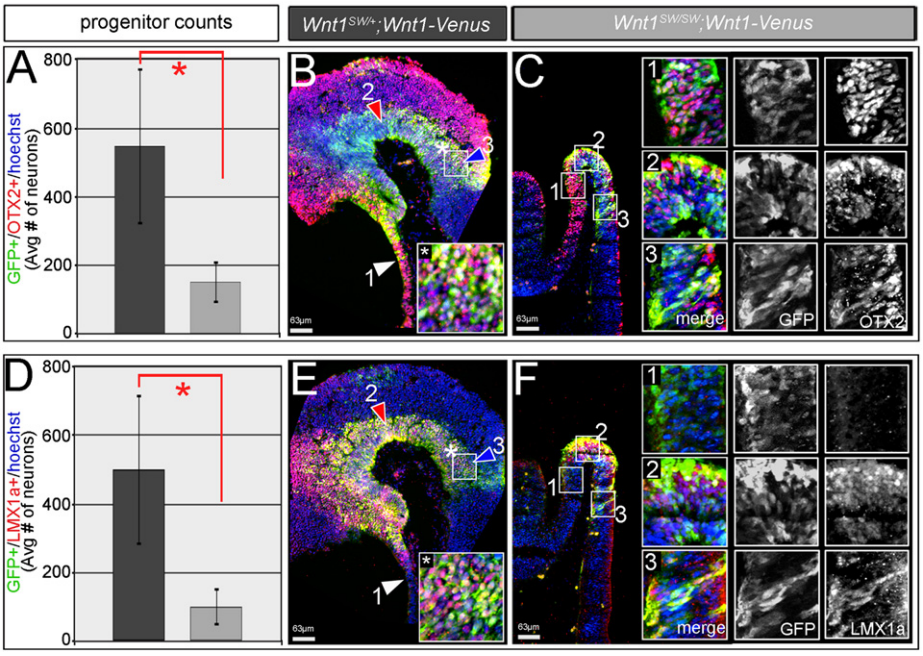

Fig. 4. Alterations in the embryonic MbDA neuron progenitors of *Wnt1*$^{SW/SW}$ embryos. The quantification and distribution of *Wnt1*(GFP)+/OTX2+ and *Wnt1*(GFP)+/LMX1a+ progenitors in the v. mes of E10.5 *Wnt1*$^{sw/+}$;*Wnt1-Venus* embryos and *Wnt1*$^{SW/SW}$;*Wnt1-Venus* littermates. (A) There was a reduction in GFP+/OTX2+ progenitors from 548 ± 228 (Ave ± SD) in controls to 152 ± 62 in mutants. (B) GFP+/OTX2+ progenitors were distributed in a well defined domain along the rostral-caudal axis in controls. Regions 1 (white arrowhead), 2 (red arrowhead), and 3 (blue arrowhead) indicate diencephalon, v. mes flexure, and caudal v. mes, respectively. Note that the *Wnt1*(GFP)+/marker+ domains are bilateral stripes (Brown et al., 2011) and one side is shown in these sagittal sections. (C) Mutants had a diminutive v. mes with mosaic clusters of *Wnt1*(GFP)+/OTX2+ mutant progenitors. (D) There was a reduction in GFP+/LMX1a+ progenitors from 501 ± 219 in controls to 101 ± 55 in mutants. (E, F) GFP+/LMX1a+ progenitors were distributed along the rostral caudal axis in controls and were diminished in mutants. Regions of interest in mutants are shown in insets 1–3 and as merged and single channels, which reveals that the caudal domain (3) has a qualitatively more striking loss of progenitors compared to the flexure (2) while domain (1) is unaffected. (For interpretation of the references to color in this figure legend, the reader is referred to the web version of this article.)

subsampled E10.5 embryos and quantified molecularly distinct progenitors in the midline and off midline domain of one side of the v. mes of sagittal sections because of clearly identifiable structures. This approach showed a similar decrease in GFP+ progenitors as determined by FACS analysis. We then addressed OTX2 expression because it functions in early MbDA neuron development. GFP+/OTX2+ progenitors were expressed broadly in the v. mes of *Wnt1*$^{SW/+}$;*Wnt1-Venus* embryos (548 ± 228, Ave ± SD) (Fig. 4A and B), which was 85% of the *Wnt1*(GFP)+ population. In contrast, GFP+/OTX2+ progenitors were reduced in *Wnt1*$^{SW/SW}$;*Wnt1-Venus* embryos (152 ± 62) (Fig. 4A and C), which was 58% of the *Wnt1*(GFP)+ population. We also assessed LMX1a, which functions as a determinant of MbDA neurons (Andersson et al., 2006) and is a direct target of *Wnt1*/β-catenin signaling (Chung et al., 2009). LMX1a+ progenitors were also expressed in progenitors located in the v. mes of wildtype embryos consistent with previous reports (Andersson et al., 2006; Sawamoto et al., 2001). In *Wnt1*$^{SW/+}$;*Wnt1-Venus* controls, GFP+/LMX1a+ progenitors (501 ± 219) made up 72% of the *Wnt1*(GFP)+ population (Fig. 4D and E). *Wnt1*$^{SW/SW}$;*Wnt1-Venus* mutants showed a significant reduction in GFP+/LMX1a+ progenitors (101 ± 55), which was only 42% of the *Wnt1*(GFP)+ population (Fig. 4D and F). Qualitatively, it appeared that the caudal v. mes was more severely affected than the v. mes flexure based on the more mosaic distribution of GFP+ cells (Compare Fig. 4C and F, regions 2 and 3). We also assessed the v. mes at E9.5, which is prior to the strong phenotype described above. *Wnt1*$^{SW/+}$;*Wnt1-Venus* embryos contained a well defined rostral OTX2+/LMX1a+ domain adjacent to an OTX2+/LMX1a+/*Wnt1*(GFP)+ domain (Supplemental Fig. 4A, A′ and C). In between the rostral and caudal domain was an intermediate OTX2+ region. In the caudal v. mes there were three adjacent regions: OTX2+/LMX1a+, OTX2+/LMX1a+/*Wnt1*(GFP)+, and OTX2+/LMX1a+ (Supplemental Fig. 4B, B′ and C). In contrast, E9.5 *Wnt1*$^{SW/SW}$;*Wnt1-Venus* embryos had a disruption of the molecularly distinct domains in the v. mes. The rostral v. mes maintained an OTX2+/LMX1a+ domain adjacent to a shrunken OTX2+/LMX1+/*Wnt1*(GFP)+ domain (Supplemental Fig. 4D, D′ and F); small clusters of OTX2+/*Wnt1*(GFP)+ cells were interspersed in this region. In contrast, the caudal v. mes was more significantly affected as evident by a near complete loss of all three caudal zones (Supplemental Fig. 4E, E′ and F). Thus, the cellular perturbation of the v. mes due to the *Wnt1*$^{SW/SW}$ mutation was first observed at E9.5 and was substantial at E10.5.

Wnt1 is critical for maintaining mes and r1 in Wnt1$^{SW/SW}$ *embryos*

We performed *in situ* hybridization to delineate changes in the patterning of the mes/r1 region. First we used probes that detected *Otx2* and *Hoxa2* to demarcate the posterior limit of the mes and the anterior limit of rhombomere 2; the intervening domain was the mes/r1. At E8.5, the mes/r1 was similar in wildtype and *Wnt1*$^{SW/SW}$ embryos (n=3 each genotype) (Fig. 5A, I). We confirmed the presence of the mes by analyzing *Wnt1*, which was detected with an *in situ* hybridization probe that covered the point mutation in exon 3. *Wnt1* was similarly expressed in *Wnt1*$^{+/+}$, *Wnt1*$^{SW/+}$ and *Wnt1*$^{SW/SW}$ littermates at E8.5 (n=3 each genotype) (Fig. 5B and J). These findings suggest that in contrast to *Wnt1* null embryos that have a significant loss of the mes/r1 domain at E8.5 (McMahon et al., 1992), the mes/r1 territory at E8.5 was unaffected by the point mutation (*Wnt1*^{SW} allele). MbDA neuron progenitors adjacent to the v. mes transiently respond to SHH signaling *in vivo* and *in vitro* and are induced to become MbDA neurons (Ye et al., 1998; Cheng et al., 2010; Blaess et al., 2006, 2011; Hayes et al., 2011). Therefore, we examined whether Shh expression in the ventral midline of the mes was dependent on Wnt1 with the rationale that a change in SHH could underpin the MbDA neuron phenotype in *Wnt1*$^{SW/SW}$ mice. The Shh domain in the floorplate was unaffected at E9.5 (Fig. 5C and K) (n=3), which is when MbDA neuron progenitors are dependent on SHH signaling *in vivo* (Blaess et al., 2006). Although *Wnt1*$^{SW/SW}$ embryos had developed a clearly aberrant morphology of the dorsal mes/r1 at E11.5, the *Shh* expression domain remained similar to wildtype littermates (Fig. 5C and K; insets). *Wnt1*$^{SW/SW}$ embryos at E9.5 did, however, have a range of alterations in morphology and in the genetic identity of mes/r1 cells compared to control littermates (Fig. 5D–H and L–P). *Wnt1*$^{SW/SW}$ embryos (n=5) showed that *Wnt1* expression in the ring at the posterior mes boundary and in the ventral midline was diminished compared to wildtype littermates at E9.5 (Fig. 5D and L). In addition, prominent clusters of both *Wnt1* and *Otx2* expressing cells were aberrantly located in dorsal-medial r1 (Fig. 5D versus L; E versus M; n=5 embryos for each marker), consistent with a previous report (Bally-Cuif et al., 1995). We investigated additional mes/r1 genes to identify changes in the molecular hierarchy involved in patterning these regions. *Gbx2* expression in r1 was reduced and the *En1* domain, encompassing both posterior mes and anterior r1, was diminished in *Wnt1*$^{SW/SW}$ embryos (n=3) (Fig. 5F, N and G, O). The loss of mes tissue in *Wnt1*$^{SW/SW}$ embryos was also apparent by assessing the size of the domain located between the *Pax6*-expressing diencephalon and either *Fgf8* or *Gbx2* using double *in situ* hybridization (n=3 each) (Fig. 6H and P; data not shown). The primary loss of tissue was in the dorsal mes with the isthmus organizer (IsO) being diminished (Fig. 5H and P) or abolished (data not shown) as determined by the expression of the *Fgf8* domain. Collectively, our analysis of *Wnt1*$^{SW/SW}$ mutants demonstrates that mes/r1 genes (*En1/2*, *Fgf8*, *Wnt1*, *Otx2*, *Gbx2*) were induced properly and suggested that sufficient patterning had occurred in mild *Wnt1*$^{SW/SW}$ embryos, which was permissive for viability. However, the molecular identity of the mes/r1 was not maintained at E9.5, which may have contributed to the loss of *Wnt1*-expressing progenitors and thus to the MbDA neuron phenotype.

Comparative genetics and MbDA neuron development

Because mes/r1 genes are co-dependent, are required during mes/r1 development, and are altered in *Wnt1*$^{SW/SW}$ embryos, we utilized *loxP* containing "floxed" alleles of *Gbx2*^{loxP} (Li et al., 2002), *Fgf8*^{loxP} (Chi et al., 2003), and *En1*^{loxP} (Sgaier et al., 2007) to generate viable conditional knockout (cko) mice. To conditionally delete these genes specifically in the mes/r1, we used *En1*^{Cre} mice (Kimmel et al., 2000) (See Methods for details of these lines). We also used conditional alleles of *En1*/*En2* in conjunction with *R26R*^{CreERT2} mice to temporally delete both *En1/2* genes (double cko, dko) after their combinatorial role in patterning the Mb and Cb during development (Cheng et al., 2010). The cko approaches allowed us to circumvent the difficulties that null alleles of *Gbx2*, *Fgf8*, and *En1/2* present, which is primarily the massive deletion of the mes/r1 and perinatal lethality due to the early role of these genes in specifying embryonic tissue (reviewed in Zervas et al., 2005). The cko alleles allowed us to examine whether these genes had a distinct role in MbDA neuron development. Specifically, we evaluated whether the loss of *Gbx2*, *Fgf8*, and *En1/2*, after their role in patterning (E9.5), led to the same MbDA neuron phenotype as observed in *Swaying* mutants. We first analyzed embryonic and adult *Gbx2 cko* mice because of the role of *Gbx2* in positioning the mes/r1 boundary (reviewed in Joyner et al., 2000), which segregates MbDA neurons from Hb serotonergic neurons (Zervas et al., 2004). In addition, *Gbx2* cko mice have a deletion of the medial Cb (vermis) (Li et al., 2002) similar to *Wnt1*$^{SW/SW}$ mice (Supplemental Figs. 1 and 5) (Bally-Cuif et al., 1995). However, in contrast to the loss of MbDA neurons and dopaminergic projections in *Wnt1*$^{SW/SW}$ mice and the disrupted me/r1 boundary, the

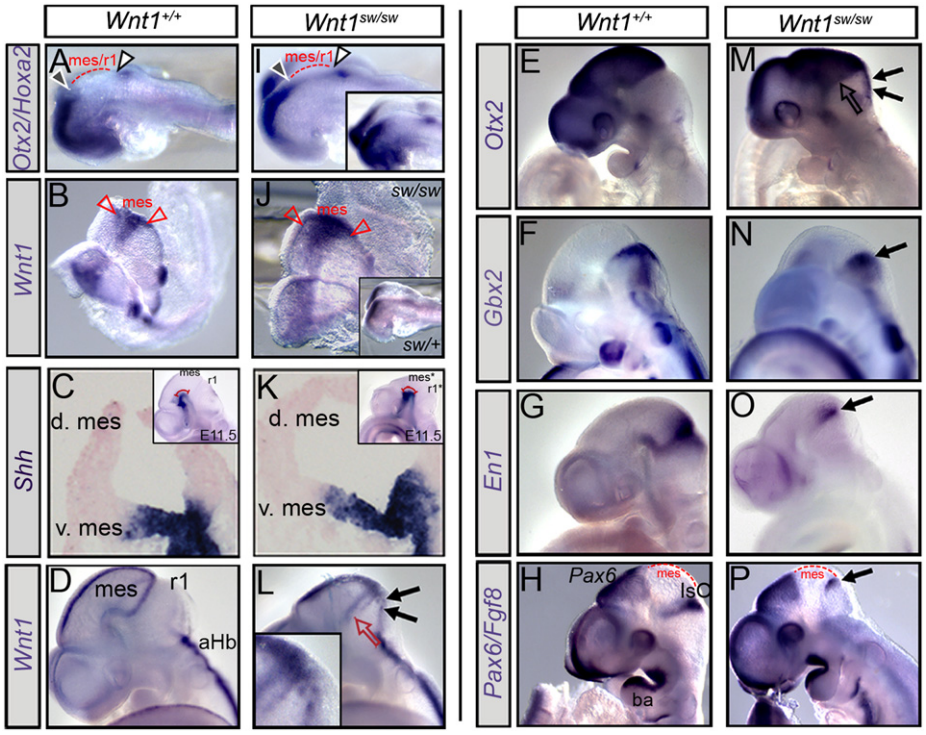

Fig. 5. Changes in the genetic identity of $Wnt1^{SW/SW}$ embryos. Wildtype versus $Wnt1^{SW/SW}$ embryos at E8.5 and E9.5 processed for whole mount *in situ* hybridization with indicated probes. (A and I) Wildtype and $Wnt1^{SW/SW}$ embryos showing the caudal limit of *Otx2*, which delineated the posterior mes (black arrowheads) while the domain between *Otx2* and *Hoxa2* corresponded to the mes/r1 (white arrowheads; *Hoxa2* delineated rhombomere 2). The mes/r1 were similar in wildtype and mutants; inset in (I) shows a second example of the double *in situ* hybridization. (B and J) *Wnt1* in the mes (red arrowheads) was indistinguishable between wildtype and $Wnt1^{SW/SW}$ embryos at E8.5; inset in (J) shows a $Wnt1^{sw/+}$ embryo that had a similar *Wnt1* expression domain as control and mutant littermates. (C, K) *Shh* expression in the v. mes of transverse sections of E9.5 wildtype and $Wnt1^{SW/SW}$ littermates; insets show *Shh* detected by wholemount *in situ* hybridization in a representative control and mutant wholemount mount embryo at E11.5. (D) The posterior limit of *Wnt1* expression was a ring shaped domain that demarcated the sharp boundary between the mes/r1. (L) In $Wnt1^{SW/SW}$ embryos the ventral domain of *Wnt1* was depleted and the posterior ring was fragmented (red arrow). In addition, clusters of *Wnt1*-expressing cells were ectopically located in dorsal-medial r1 (L, black arrows; inset shows higher magnification). (E and M) The lateral edges of the *Otx2* domain were similar between wildtype and $Wnt1^{SW/SW}$ embryos (M, open arrow) although dorsal and medial expression of *Otx2* was perturbed (M, filled arrows). (F and N) The anterior *Gbx2* expression domain that delineated r1 was depleted primarily in a dorsal domain in $Wnt1^{SW/SW}$ embryos leaving behind a patch of expression (N, arrow). (G and O) *En1* labeled the posterior mes and r1 and was significantly depleted in mutant littermates (O, arrow). (H) *Pax6* defined the anterior developing nervous system and caudally indicated the interface between the posterior diencephalon and anterior mes. *Fgf8* was expressed in anterior r1 (isthmus organizer, IsO). The unmarked domain between *Pax6* and *Fgf8* was the mes. (P) In $Wnt1^{SW/SW}$ embryos the *Pax6* domain was unaffected while the IsO was substantially reduced (P, arrow). The mes in between *Pax6* and *Fgf8* was diminished. (For interpretation of the references to color in this figure legend, the reader is referred to the web version of this article.)

conditional gene deletion of *Gbx2* ($n=3$) did not overtly affect the position of MbDA neurons during embryogenesis, the distribution of adult MbDA neurons, or the innervation of MbDA neuron targets (Supplemental Fig. 5).

Fgf8 is expressed in the isthmus from E8.5–E12.5 and it has been previously shown that the conditional deletion of *Fgf8* in $En1^{Cre}$;$Fgf8^{loxP/loxP}$ mice results in the loss of the Mb including MbDA neurons at E18.5 (Chi et al., 2003). It was proposed that the loss of MbDA neurons was due to the lack of MbDA neuron induction, which was consistent with the early and transient role of *FGF8* in inducing MbDA neurons *in vitro* (Ye et al., 1998). However, MbDA neurons were not assessed at early stages in *Fgf8* cko mice leaving open the possibility that MbDA neurons had been induced and then depleted by the end of embryogenesis. Therefore, we re-visited this issue to determine whether MbDA neurons had been induced *in vivo* in E12.5 *Fgf8* cko embryos. The conditional removal of *Fgf8* mediated by $En1^{Cre}$ resulted in the ablation of the dorsal mes and r1 at E12.5 although ventral tissue was less severely affected (Fig. 6A and D). Interestingly, we observed a similar pattern and positioning of MbDA neurons in wildtype and *Fgf8* cko mice at E12.5 (Fig. 6B and E; $n=3$). However, all MbDA neurons were gone at E18.5, consistent with previous reports (data not shown, see Chi et al., 2003). LMX1a+ MbDA neuron progenitors were present and were distributed in a qualitatively similar manner in control and *Fgf8* cko embryos at E12.5 (Fig. 6C and F; $n=3$). Therefore, while *Fgf8* cko mice had a severely ablated mes/r1, the deletion of *Fgf8* after E9.0 did not impact the presence of LMX1a+ progenitors and did not prevent the induction of TH+ MbDA neurons. Although *Fgf8* cko did not mimic the depletion of LMX1a+ MbDA neuron progenitors seen in $Wnt1^{SW/SW}$ mutants, the loss of MbDA neurons after their induction may suggest that changes in *Fgf8* could be a contributing factor to the $Wnt1^{SW/SW}$ phenotype and that there is a late requirement for *Fgf8* in MbDA neuron survival.

We took advantage of *En1* cko and *En1/2* dcko mice to address the temporal role of the *Engrailed* genes, which were affected in $Wnt1^{SW/SW}$ embryos. $En1^{Cre}$;$En1^{loxP}$ (*En1* cko) mice have a truncated tectum, although 20% of the mice have a normal cerebellum (Sgaier et al., 2007). In E11.5 embryos that had *En1* conditionally removed after E9.0, MbDA neurons were present in the v. mes and distributed in a similar pattern as controls although the v. mes was smaller in cko embryos (Supplemental Fig. 6A and B; $n=3$). However, even when the posterior mes and r1 were entirely missing in *En1* cko embryos, MbDA neurons were still present, but they were subtly diminished in the v. mes (Supplemental Fig. 6C and D). Adult *En1* cko mice were viable and had VTA and SNc MbDA neurons although the SNc was diminished compared to wildtype controls (compare Supplemental Fig. 6E–G with Fig. 1A–C). *En1/2* double knockout mice (null alleles)

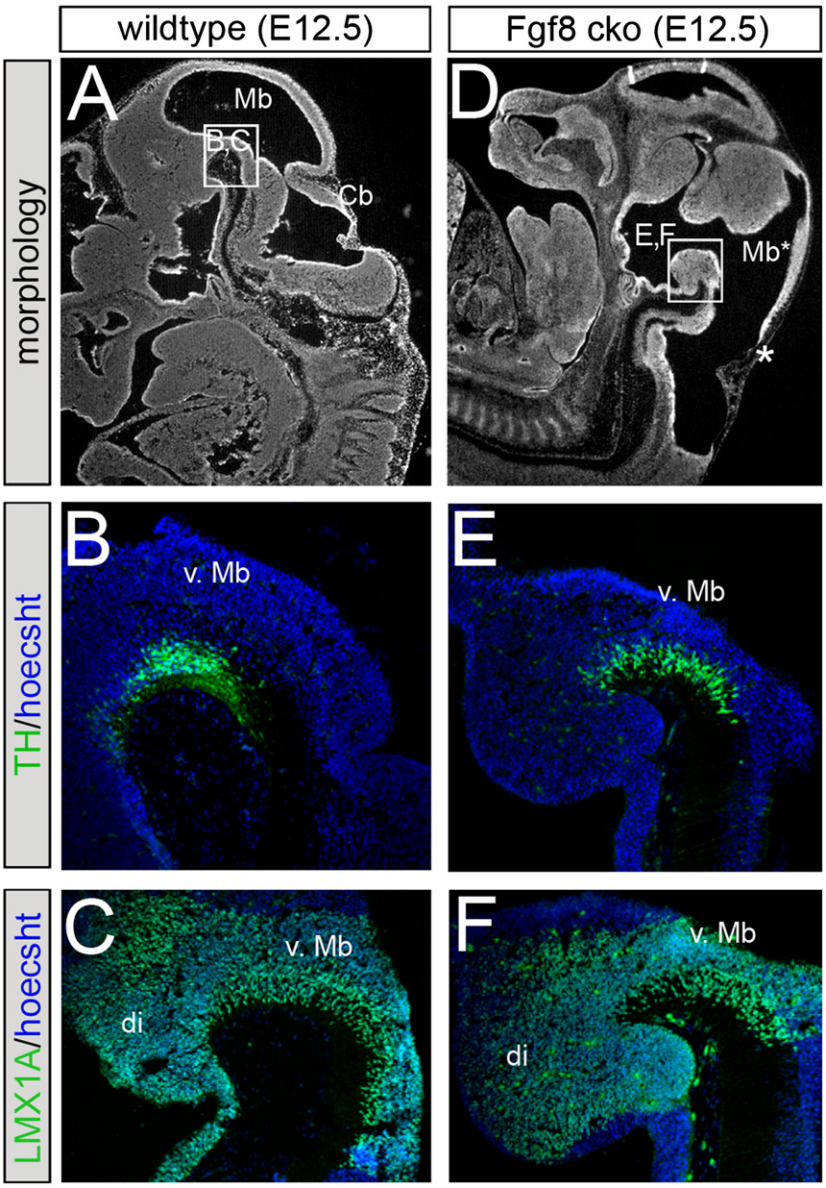

Fig. 6. MbDA neuron induction was independent of *Fgf8* after E9.0. (A and D) Sagittal sections of E12.5 wildtype and *Fgf8* cko embryos counterstained with hoechst showing overview of embryonic morphology and the region where TH$^+$ MbDA neurons and LMX1a$^+$ progenitors were located. *Fgf8* cko embryos had a deletion of the posterior Mb (Mb*) and Cb. (B and E) Wildtype differentiating MbDA neurons resided in the v. Mb while *Fgf8* cko littermates had MbDA neurons that were loosely organized and subtly diminished. (C and F) LMX1a+ progenitors were expressed in the v. Mb similarly between wildtype and mutants. B and C are near adjacent sections and E and F are adjacent sections.

have a complete loss of Mb and aHb at E14.5 precluding the ability to assess a later temporal role in MbDA neuron development (Simon et al., 2004). To determine whether *En1*/*En2* continued to play a combinatorial role in MbDA neuron development we temporally deleted by administering tamoxifen to E10.5 $R26R^{CreERT2}$;$En1^{lox/-}$;$En2^{GFPloxP/-}$ embryos (Cheng et al., 2010) (Fig. 7). We used a pan-EN antibody and TH immunolabeling to ascertain the distribution of MbDA neurons expressing EN protein in wildtype embryos (Fig. 7A and B). The result of inactivating both *En1*/*2* caused a near complete ablation of MbDA neurons at E17.5 embryos, which we validated with EN/TH immunolabeling ($n=3$) (Fig. 7C and D). In contrast to $Wnt1^{SW/SW}$ mice, there was not a biased loss of the medial-lateral MbDA neurons. The CreER system is mosaic in mediating recombination (Joyner and Zervas, 2006), which likely accounted for the surviving MbDA neurons, which expressed EN (Fig. 7C and D).

En2 rescues the dorsal Mb and Cb morphological phenotype in the absence of En1, but MbDA neurons were not assessed in either of these studies (Hanks et al., 1995; Sgaier et al., 2007). To directly test whether *En2* itself was sufficient for MbDA neuron development/survival we used a combination of null alleles and species-specific knock-in alleles (Fig. 8). Compared to wildtype mice at birth, mice that had murine *En2* knocked into the *En1* locus ($En1^{En2/En2}$) had a morphologically wildtype Mb and Cb consistent with previous reports (Hanks et al., 1995; Sgaier et al., 2007). We found that $En1^{En2/En2}$ mice had a normal compliment of MbDA neurons at birth (data not shown). MbDA neuron populations also appeared normal in mice that had *En2* knocked into the *En1* locus even when on an *En2* null mutant background ($En1^{En2/En2}$;$En2^{-/-}$) (Fig. 8A–D; $n=3$). In contrast, replacing mouse *En1* with *Drosophila en* (*Den*) on the *En2* null background ($En1^{Den/Den}$;$En2^{-/-}$) resulted in a near complete loss of MbDA neurons

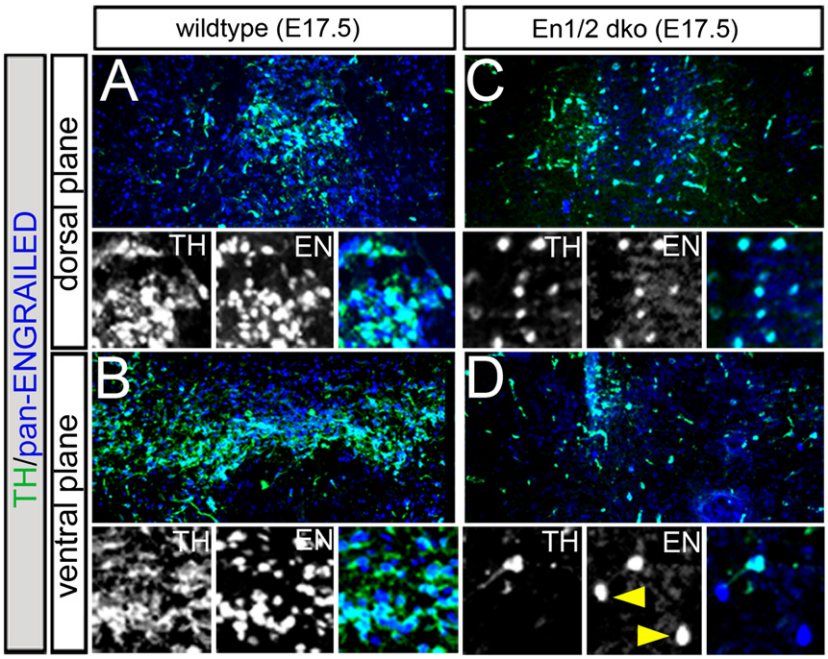

Fig. 7. Double conditional knockout (dko) of *En1* and *En2*. EN protein detected with a pan-Engrailed antibody (blue) in horizontal sections. $R26R^{CreERT2}$;$En1^{lox/-}$;$En2^{GFPlox/-}$ mice were given tamoxifen at E10.5 to delete *En1/2* and were analyzed at E17.5. (A) Medial MbDA neurons (green) expressing EN in a dorsal section. (B) EN in VTA/SNc MbDA neurons in a more ventral section. Panels below (A) and (B) show high magnification images of TH+ and EN+ cells in their respective single channel. TH/EN labeling were merged in the color panels. MbDA neurons expressed EN protein in nucleus-like staining. (C and D) *En1/2* dko mice had decreased MbDA neurons in dorsal VTA and a substantial depletion of MbDA neurons in the VTA/SNc ventrally. Panels below (C) and (D) show examples of neurons expressing the indicated antigens in single channel and in combined images. Note that nearly all of the remaining MbDA neurons in *En1/2* cko mutants still expressed EN. The panels under (D) show a few EN expressing cells that did not have TH labeling (yellow arrowheads) and serve as an internal control for the specificity of the antibody labeling. (For interpretation of the references to color in this figure legend, the reader is referred to the web version of this article.)

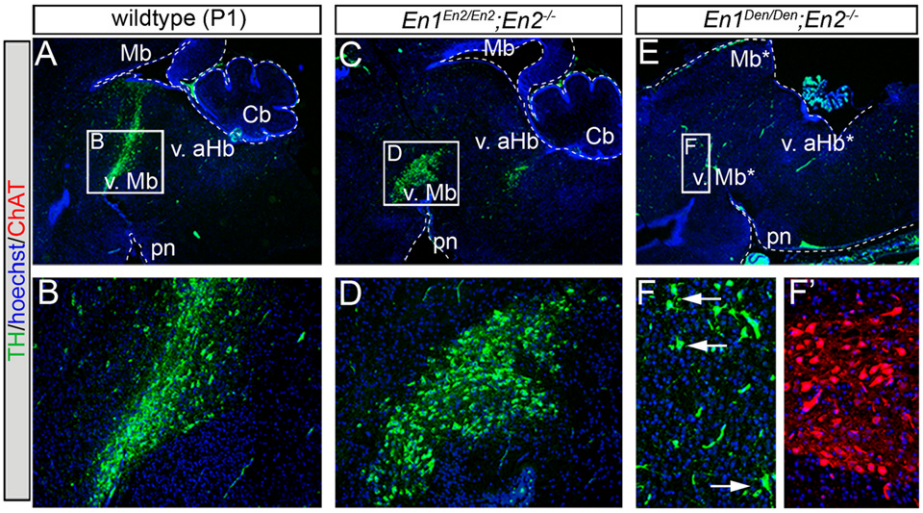

Fig. 8. Species-specific role of *Engrailed* genes in MbDA neuron development. (A and B) Wildtype sagittal sections showing MbDA neurons at birth. (C and D) Sagittal section of mouse pup with *En2* knocked in to the *En1* locus on an *En2* null background ($En1^{En2/En2}$;$En2^{-/-}$) showing a similar distribution of MbDA neurons versus control littermates. (E–F′) *Drosophila en (Den)* knocked into the *En1* locus on the $En2^{-/-}$ background ($En1^{Den/Den}$;$En2^{-/-}$) did not rescue MbDA neurons which were largely depleted; note also the severe loss of dorsal Mb (Mb*) and absence of Cb. The choroid plexus (cp), is still distinguishable as was the pontine nucleus (pn). A few remaining MbDA neurons were observed (F, arrows) while cholinergic neurons (F′, $ChAT^+$, red) were seen in the truncated aHb (*).

(Fig. 8E and F $n=3$), but not cholinergic neurons of the LDTg (Fig. 8F′). Collectively, these data show that the mouse *Engrailed* genes function in MbDA neuron development after E10.5 and that the continued presence of mouse *En2* alone, but not *Den*, is sufficient to drive the process of MbDA neuron development *in vivo*. Thus, there is a temporal and species-specific requirement for Engrailed genes in MbDA neuron development.

Discussion

Wnt1-expressing progenitors in the v. mes contribute to MbDA neurons *in vivo* (Zervas et al., 2004; Brown et al., 2011). However, determining the functional requirement of *Wnt1* in MbDA neurons *in vivo* has been enigmatic because of extensive Mb deletion and lethality in *Wnt1* null mice (McMahon and Bradley,

1990). Analyzing adult *Wnt1*$^{SW/SW}$ mice circumvents these problems and reveals that *Wnt1* is critical to the development of TH+/CALB+ MbDA neurons of the VTA and to a lesser although substantial extent of the SNc. Regardless, *Wnt1*$^{SW/SW}$ mice are a rare example of a phenotype involving the complete depletion of VTA MbDA neurons and thus represents a valuable research tool for the Neuroscience community. We show that *Wnt1*(GFP) mutant progenitors are significantly depleted in *Wnt1*$^{SW/SW}$ embryos prior to MbDA neuron differentiation. The caudal OTX2+/LMX1a+/*Wnt1*(GFP)+ progenitors are the most severely affected suggesting that these depleted progenitors correspond to VTA MbDA neurons. In contrast, the remaining progenitors likely correspond to surviving SNc MbDA neurons (Fig. 9A). The deletion of *Otx2* at E9.0 using *En1*^{Cre} or mutations in *Lmx1a* cause a global reduction of MbDA neurons (Puelles et al., 2004; Chung et al., 2009). However, recent studies have shown that OTX2 loss or gain of function strongly influences more caudal MbDA progenitors (Omodei et al., 2008) and that OTX2 continues to be required for a subset of VTA (dorsal-lateral VTA) MbDA neurons (Di Salvio et al., 2010). Our findings augment these reports and suggest that *Wnt1* is also critical for a subset of MbDA neuron progenitors, with a strong bias toward LMX1a-expressing progenitors corresponding to the entire VTA, including the most medial VTA. This finding is consistent *Wnt1*/β-catenin signaling that culminates in ß-catenin nuclear translocation and binding to *Lmx1a* (Chung et al., 2009). In addition, *Lmx1a* binds directly to the *Wnt1* promoter of cells from v. mes tissue as part of a *Wnt1-Lmx1a* reciprocal regulatory loop (Chung et al., 2009). Our finding that LMX1a+ progenitors are diminished, but not abolished, in *Wnt1*$^{SW/SW}$ embryos further suggests that *Wnt1*-independent pathways also regulate MbDA neuron progenitors. *Shh* is expressed in the v. mes and Shh signaling is required to induce TH+ neurons from v. mes progenitors (Ye et al., 1998; Blaess et al., 2006). Interestingly, the *Shh* domain is not diminished in *Wnt1*$^{SW/SW}$ homozygotes indicating that *Wnt1* is not required to regulate or maintain *Shh* expression and that the depletion of *Wnt1*(GFP)+ and LMX1a+ progenitors occurs independent of *Shh*. Our *in vivo* data complements stem cell studies showing the *Wnt1-LMX1a* loop does not require SHH signaling (Chung et al., 2009). Therefore, multiple genetic components influence the MbDA progenitor pool.

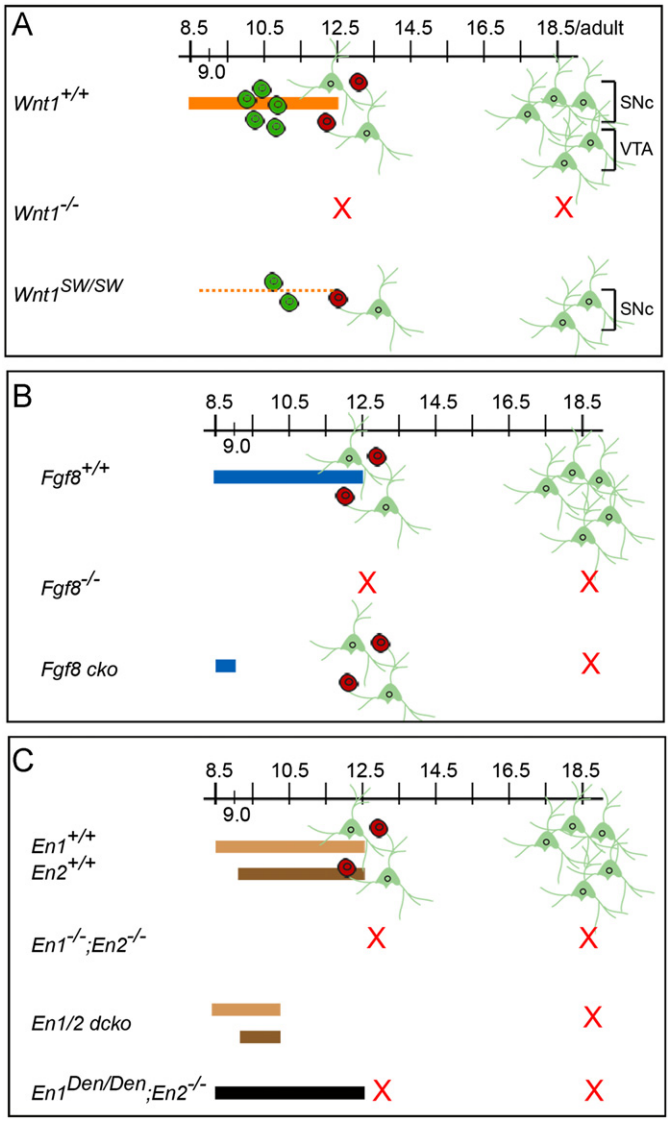

Fig. 9. Summary Schematic of MbDA neuron phenotypes. (A) The expression of *Wnt1* (orange bar) and the distribution of *Wnt1*(GFP)$^{+}$ progenitors (green circles), LMX1a^{+} progenitors (red circles), and MbDA neurons (green neurons) at key developmental stages in *Wnt1*$^{+/+}$, *Wnt1*$^{-/-}$, and *Wnt1*$^{SW/SW}$ mice. (B) The expression of *Fgf8* (blue bar) and the distribution of LMX1a+ progenitors and MbDA neurons at key developmental stages in *Fgf8*$^{+/+}$, *Fgf8*$^{-/-}$, and *Fgf8 cko* mice. (C) The expression of *En1* (tan bar) and *En2* (brown bar) and the distribution of LMX1a+ progenitors and MbDA neurons at key developmental stages in *En1*$^{+/+}$;*En2*$^{+/+}$, *En1*$^{-/-}$;*En2*$^{-/-}$, *En1/En2 dcko*, and *En1*$^{Den/Den}$;*En2*$^{-/-}$ mice. The black brown bar indicates *Drosophila engrailed*. (For interpretation of the references to color in this figure legend, the reader is referred to the web version of this article.)

The *Wnt1*$^{SW/SW}$ mutation not only results in the biased loss of VTA, but also results in the mixing of remaining medial MbDA neurons and serotonin neurons. Our studies indicate that the mixing of TH+/5HT+ progenitors in *Wnt1*$^{SW/SW}$ embryos occurs prior to E9.0. These populations are normally segregated during development by a v. mes lineage restriction boundary (Zervas et al., 2004). Our current study shows that the ventral mes/r1 lineage boundary depends on functional *Wnt1*, which augments previous findings that the dorsal mes/r1 boundary also requires the presence of *Wnt1* (Bally-Cuif, 1995) Interestingly, the fidelity of the patterned domains in *Wnt1*$^{SW/SW}$ embryos appears normal at E8.5 indicating that the induction of mes/r1 gene expression and the establishment of the ventral lineage boundary *in vivo* may be linked through *Wnt1* between E8.5 and E9.0. Collectively our results suggest that a biased loss of MbDA neurons could be the result of a complex set of interrelated mechanisms gone awry in *Wnt1*$^{SW/SW}$ embryos where the loss of some caudal v. mes progenitors coupled with a mixing of remaining caudal v. mes and rostral v. r1 progenitors might deplete the VTA pool while leaving intact a more rostrally located SNc (TH+/Calb+) progenitor pool.

The genetic hierarchy of mes/r1 genes are compromised at time points consistent with the induction and maintenance of additional genes in the mes/r1 (Li and Joyner, 2001). Because mes/r1 genetic identity is not properly maintained by E9.5 in *Wnt1*$^{SW/SW}$ embryos, we addressed the degree of involvement of additional mes/r1 genes using conditional mutant lines. *Fgf8* is diminished in *Wnt1*$^{SW/SW}$ embryos but *Fgf8* cko embryos that underwent *En1*^{Cre}-mediated deletion (after E9.0) reveals that LMX1a-expressing progenitors and differentiating MbDA neurons are largely unaffected at E12.5 (Fig. 9B). Collectively, these findings suggest that induction of MbDA neuron progenitors requires *Wnt1* during a transient window (prior to E9.0) coincident with *Fgf8*. This idea is supported by *in vitro* findings (Ye et al., 1998) and *Wnt1*$^{-/-}$ explants in which *Wnt1* is necessary for *Fgf8*-mediated induction of ectopic MbDA neurons (Prakash et al., 2006). Interestingly, it was previously shown that the deletion of *Fgf8* at E9.0 with *En1*^{Cre} deleter mice results in a complete absence of MbDA neurons at E18.5, which we also observed (data not shown) (Chi et al., 2003). Therefore, our results clarify that *Fgf8* plays an additional role between E9.0 and the time when *Fgf8*

expression is extinguished (E12.5) to ensure the continued survival of MbDA neurons after *Fgf8* is no longer expressed. FGF ligands physically interact with and signal through the 'c' isoforms of three FGF receptors, *Fgfr1*, *Fgfr2* and *Fgfr3* (Olsen et al., 2006). The conditional inactivation of *Fgfr1* and *Fgfr2* using $En1^{Cre}$ showed a depletion of MbDA neurons (Saarimaki-Vire et al., 2007). The phenotype worsened when *Fgfr1*, and *Fgfr2* were conditionally removed on an *Fgfr3* null background. Collectively, these findings suggest that *FGF8* is responsible for multiple phases of MbDA neuron development likely by signaling through all three Fgfr receptors.

En1 null mice have a deletion of the Mb/aHb by E9.5, which results in perinatal lethality and disorganization of MbDA neurons at E18.5 (Wurst et al., 1994). The expression of En1 precedes En2 by approximately 12 h (Joyner, 2000) and during this early period the *En* genes are necessary to pattern the mes (Hanks et al., 1995; Sgaier et al., 2007; Cheng et al., 2010). *En1*/*En2* have a gene dosage requirement for MbDA neuron survival (Simon et al., 2001) although the temporal component of the gene dosage effect has not been determined. We inactivated the *En* genes after their early requirement to better understand the extent of *En* function in MbDA development. Deleting *En1*/*En2* at E10.5 causes a severe loss of MbDA neurons (Fig. 9C). Interestingly, MbDA neurons that survive, because of the mosaic nature of CreER mediated recombination (Joyner Zervas, 2006), still express EN protein. This *in vivo* genetic evidence suggests that both *Engrailed* genes are required cell autonomously for MbDA neuron survival, which is in agreement with cell mixing experiments of *En* double mutant cells with wildtype mes cells (Alberi et al., 2004). $En1^{En2/En2}$; $En2^{-/-}$ mice have a wildtype MbDA neuron distribution pattern indicating that two copies of *En2* are solely sufficient to direct MbDA neuron development. Notably, MbDA neuron development was drastically reduced in $En1^{Den/\ Den}$;$En2^{-/-}$ mice in which two copies of *Den* are expressed in the absence of both mouse *En* genes (Fig. 9C). Interestingly, *Den* alone is unable to support MbDA neuron development. Thus, we show the specificity and evolutionary distinctions of EN protein function in MbDA neuron development (Fig. 9C).

The comparative genetics of $Wnt1^{SW/SW}$ embryos versus *Gbx2*, *Fgf8*, and *En1*/*2* conditional mutant embryos reveals that *Wnt1* is unique in its requirement for VTA MbDA neurons and that these genes may play distinct roles in MbDA neuron development. However, we do not rule out that these genes may work cooperatively in the MbDA neuron development, which this analysis could not resolve. Interestingly, the loss of VTA MbDA neurons was concomitant with the loss of innervation of the BNST. MbDA neuron innervation of target sites during development has been proposed to occur by a mechanism that uses promiscuous innervation of targets and selective refinement (Hu et al., 2004). Because the loss of VTA occurs during early development, it might have been predicted that remaining MbDA neurons innervate a broader selection of targets. However, the remaining SNc MbDA neurons in $Wnt1^{SW/SW}$ mice do not form connections to some VTA targets as exemplified by the lack of dopamine innervation of the bed nucleus even though this target is present and replete with cholinergic neurons. These findings indicate that the development of the VTA and its targets are uncoupled. The loss of VTA MbDA neurons are likely to contribute to the motor behavior abnormalities in $Wnt1^{SW/SW}$ mice although these defects have generally been attributed to alterations in the medial region of the Cb (vermis) (Lane, 1967; Thomas et al., 1991). We cannot rule out that the vermis phenotype contributes to the behavioral deficits in $Wnt1^{SW/SW}$ mice. However, the lack of a motor deficit in *Gbx2* cko mice (Movie 3), which have a vermis deletion (Li et al., 2002) without the lack of overt MbDA neuron loss suggests that the $Wnt1^{SW/SW}$ phenotype is the result of MbDA neuron loss. Our findings of primarily VTA MbDA neuron involvement are interesting in the broader context of movement disorders. Parkinson's disease is typically attributed to SNc MbDA neuron loss (Parent, 1996), but is often accompanied by VTA loss (Damier et al., 1999; Hirsch et al., 1988; Uhl et al., 1985). Additionally, movement deficits in Parkinsonian animal models either worsen or unique deficits appear when VTA DA neurons are compromised (Heim et al., 2002; Moore et al., 2001). This is likely because of the VTA involvement in planning, initiation, and motivation of movement (Uhl et al., 1985). In summary, our results complement previous results describing that the acquisition of *Wnt1* expression is a part of the molecular profile that occurs during the programming of embryonic stem cells to acquire a MbDA neuron fate (Lee et al., 2000). Furthermore, our findings provide new insight into the developmental genetic program underpinning VTA MbDA neuron development.

Supplementary material related to this article can be found online at doi:10.1016/j.ydbio.2012.09.019.

Acknowledgments

The initial genetic analysis and *Fgf8* and *En1*/*2* cko analysis was performed my MZ while a postdoctoral fellow in Alexandra L. Joyner's lab. Subsequent analysis of mutants and FACS was done by DE, CR, BV in the laboratory of Mark Zervas at Brown University. A portion of these studies were funded by an NIH fellowship (F32 HD043533, MZ). FACS analysis and the molecular identity of *Wnt1*-expressing progenitors was funded by startup funds and a Brown University Solomon award (MZ). A portion of these studies was funded by RI COBRE Hospital Center for Stem Cell Biology award (P20RR025179-02, sub-award #701-1960, MZ project leader).

Appendix A. Supporting information

Supplementary data associated with this article can be found in the online version at http://dx.doi.org/10.1016/j.ydbio.2012.09.019

References

Alberi, L., Sgado, P., Simon, H.H., 2004. Engrailed genes are cell-autonomously required to prevent apoptosis in mesencephalic dopaminergic neurons. Development 131, 3229–3236.

Andersson, E., Tryggvason, U., Deng, Q., Friling, S., Alekseenko, Z., Robert, B., Perlmann, T., Ericson, J., 2006. Identification of intrinsic determinants of midbrain dopamine neurons. Cell 124, 393–405.

Bally-Cuif, L., Cholley, B., Wassef, M., 1995. Involvement of *Wnt-1* in the formation of the mes/metencephalic boundary. Mech. Dev. 53, 23–34.

Berendse, H.W., Galis-de Graaf, Y., Groenewegen, H.J., 1992. Topographical organization and relationship with ventral striatal compartments of prefrontal corticostriatal projections in the rat. J. Comp. Neurol. 316, 314–347.

Blaess, S., Bodea, G.O., Kabanova, A., Chanet, S., Mugniery, E., Derouiche, A., Stephen, D., Joyner, A.L., 2011. Temporal–spatial changes in Sonic Hedgehog expression and signaling reveal different potentials of ventral mesencephalic progenitors to populate distinct ventral midbrain nuclei. Neural Dev. 6, 29.

Blaess, S., Corrales, J.D., Joyner, A.L., 2006. Sonic hedgehog regulates Gli activator and repressor functions with spatial and temporal precision in the mid/hindbrain region. Development 133, 1799–1809.

Brown, A., Brown, S., Ellisor, D., Hagan, N., Normand, E., Zervas, M., 2009. A practical approach to genetic inducible fate mapping: a visual guide to mark and track cells *in vivo*. J. Vis. Exp. pii, 1687.

Brown, A., Machan, J.T., Hayes, L., Zervas, M., 2011. Molecular organization and timing of *Wnt1* expression define cohorts of midbrain dopamine neuron progenitors *in vivo*. J. Comp. Neurol. 519, 2978–3000.

Castelo-Branco, G., Wagner, J., Rodriguez, F.J., Kele, J., Sousa, K., Rawal, N., Pasolli, H.A., Fuchs, E., Kitajewski, J., Arenas, E., 2003. Differential regulation of midbrain dopaminergic neuron development by *Wnt-1*, *Wnt-3a*, and *Wnt-5a*. Proc. Natl. Acad. Sci. USA 100, 12747–12752.

Chang, H.T., 1988. Dopamine-acetylcholine interaction in the rat striatum: a dual-labeling immunocytochemical study. Brain. Res. Bull. 21, 295–304.

Cheng, Y., Sudarov, A., Szulc, K.U., Sgaier, S.K., Stephen, D., Turnbull, D.H., Joyner, A.L., 2010. The Engrailed homeobox genes determine the different foliation patterns in the vermis and hemispheres of the mammalian cerebellum. Development 137, 519–529.

Chi, C.L., Martinez, S., Wurst, W., Martin, G.R., 2003. The isthmic organizer signal FGF8 is required for cell survival in the prospective midbrain and cerebellum. Development 130, 2633–2644.

Chung, S., Leung, A., Han, B.S., Chang, M.Y., Moon, J.I., Kim, C.H., Hong, S., Pruszak, J., Isacson, O., Kim, K.S., 2009. *Wnt1*-lmx1a forms a novel autoregulatory loop and controls midbrain dopaminergic differentiation synergistically with the SHH-FoxA2 pathway. Cell. Stem. Cell. 5, 646–658.

Damier, P., Hirsch, E.C., Agid, Y., Graybiel, A.M., 1999. The substantia nigra of the human brain. II. Patterns of loss of dopamine-containing neurons in Parkinson's disease. Brain 122, 1437–1448, Pt 8.

Di Salvio, M., Di Giovannantonio, L.G., Acampora, D., Prosperi, R., Omodei, D., Prakash, N., Wurst, W., Simeone, A., 2010. Otx2 controls neuron subtype identity in ventral tegmental area and antagonizes vulnerability to MPTP. Nat. Neurosci. 13, 1481–1488.

Ellisor, D., Koveal, D., Hagan, N., Brown, A., Zervas, M., 2009. Comparative analysis of conditional reporter alleles in the developing embryo and embryonic nervous system. Gene. Expr. Patterns. 9, 475–489.

Fay, M.P., Graubard, B.I., 2001. Small-sample adjustments for wald-type tests using sandwich estimators. Biometrics 57, 1198–1206.

Fallon, J.H., Opole, I.O., G., P.S., 2003. The neuroanatomy of schizophrenia: circuitry and neurotransmitter systems. Clin. Neurosci. Res. 3, 77–107.

Gaykema, R.P., Zaborszky, L., 1996. Direct catecholaminergic-cholinergic interactions in the basal forebrain. II. Substantia nigra-ventral tegmental area projections to cholinergic neurons. J. Comp. Neurol. 374, 555–577.

Georges, F., Aston-Jones, G., 2002. Activation of ventral tegmental area cells by the bed nucleus of the stria terminalis: a novel excitatory amino acid input to midbrain dopamine neurons. J. Neurosci. 22, 5173–5187.

Gerfen, C.R., Baimbridge, K.G., Thibault, J., 1987. The neostriatal mosaic: III. Biochemical and developmental dissociation of patch-matrix mesostriatal systems. J. Neurosci. 7, 3935–3944.

Goridis, C., Rohrer, H., 2002. Specification of catecholaminergic and serotonergic neurons. Nat. Rev. Neurosci. 3, 531–541.

Grimm, J., Mueller, A., Hefti, F., Rosenthal, A., 2004. Molecular basis for catecholaminergic neuron diversity. Proc. Natl. Acad. Sci. USA 101, 13891–13896.

Hagan, N., Zervas, M., 2012. *Wnt1* expression temporally allocates upper rhombic lip progenitors and defines their terminal cell fate in the cerebellum. Mol. Cell. Neurosci 49, 217–229.

Hanks, M., Wurst, W., Anson-Cartwright, L., Auerbach, A.B., Joyner, A.L., 1995. Rescue of the En-1 mutant phenotype by replacement of En-1 with En-2. Science 269, 679–682.

Hanks, M.C., Loomis, C.A., Harris, E., Tong, C.X., Anson-Cartwright, L., Auerbach, A., Joyner, A., 1998. Drosophila engrailed can substitute for mouse Engrailed1 function in mid-hindbrain, but not limb development. Development 125, 4521–4530.

Hasue, R.H., Shammah-Lagnado, S.J., 2002. Origin of the dopaminergic innervation of the central extended amygdala and accumbens shell: a combined retrograde tracing and immunohistochemical study in the rat. J. Comp. Neurol. 454, 15–33.

Hayes, L., Zhang, Z., Albert, P., Zervas, M., Ahn, S., 2011. The timing of Sonic hedgehog and Gli1 expression segregates midbrain dopamine neurons. J. Comp. Neurol. 519, 3001–3018.

Heim, C., Sova, L., Kurz, T., Kolasiewicz, W., Schwegler, H., Sontag, K.H., 2002. Partial loss of dopaminergic neurons in the substantia nigra, ventrotegmental area and the retrorubral area -model of the early beginning of Parkinson's symptomatology? J. Neural. Transm. 109, 691–709.

Hinkley, D.V., 1977. Jackknifing in Unbalanced situations. Technometrics 19, 285–292.

Hirsch, E., Graybiel, A.M., Agid, Y.A., 1988. Melanized dopaminergic neurons are differentially susceptible to degeneration in Parkinson's disease. Nature 334, 345–348.

Hu, Z., Cooper, M., Crockett, D.P., Zhou, R., 2004. Differentiation of the midbrain dopaminergic pathways during mouse development. J. Comp. Neurol. 476, 301–311.

Huber, P.J., 1967. The behavior of maximum likelihood estimates under nonstandard conditions. In: Proceedings of the Fifth Berkeley Symposium on Mathematical Statistics and Probability. vol. 1, pp. 221–233.

Joyner, A.L., 2000. Gene Targeting: A Practical Approach. Oxford University Press, Oxford, New York.

Joyner, A.L., Liu, A., Millet, S., 2000. *Otx2*, *Gbx2* and *Fgf8* interact to position and maintain a mid-hindbrain organizer. Curr. Opin. Cell. Biol. 12, 736–741.

Joyner, A.L., Zervas, M., 2006. Genetic inducible fate mapping in mouse: Establishing genetic lineages and defining genetic neuroanatomy in the nervous system. Dev. Dyn. 235, 2376–2385.

Kimmel, R.A., Turnbull, D.H., Blanquet, V., Wurst, W., Loomis, C.A., Joyner, A.L., 2000. Two lineage boundaries coordinate vertebrate apical ectodermal ridge formation. Genes. Dev. 14, 189–1377.

Kauermann, G., Carroll, R.J., 2001. A Note on the Efficiency of Sandwich Covariance Estimation. J. Am. Stat. Assoc. 96, 1387–1396.

Kubota, Y., Inagaki, S., Shimada, S., Kito, S., Eckenstein, F., Tohyama, M., 1987. Neostriatal cholinergic neurons receive direct synaptic inputs from dopaminergic axons. Brain. Res. 413, 179–184.

Lane, P.W., 1967. [Swaying]. Mouse News. Lett, 40.

Lee, S.H., Lumelsky, N., Studer, L., Auerbach, J.M., McKay, R.D., 2000. Efficient generation of midbrain and hindbrain neurons from mouse embryonic stem cells. Nat. Biotechnol. 18, 675–679.

Li, J.Y., Joyner, A.L., 2001. *Otx2* and *Gbx2* are required for refinement and not induction of mid- hindbrain gene expression. Development 128, 491–4979.

Li, J.Y., Lao, Z., Joyner, A.L., 2002. Changing requirements for *Gbx2* in development of the cerebellum and maintenance of the mid/hindbrain organizer. Neuron. 36, 31–43.

Manger, P.R., Fahringer, H.M., Pettigrew, J.D., Siegel, J.M., 2002. The distribution and morphological characteristics of serotonergic cells in the brain of monotremes. Brain. Behav. Evol. 60, 315–332.

McMahon, A.P., Bradley, A., 1990. The Wnt-1 (int-1) proto-oncogene is required for development of a large region of the mouse brain. Cell 62, 1073–1185.

McMahon, A.P., Joyner, A.L., Bradley, A., McMahon, J.A., 1992. The midbrain-hindbrain phenotype of Wnt-1-/Wnt-1- mice results from stepwise deletion of engrailed-expressing cells by 9.5 days postcoitum. Cell 69, 581–595.

Mendez, I., Sanchez-Pernaute, R., Cooper, O., Vinuela, A., Ferrari, D., Bjorklund, L., Dagher, A., Isacson, O., 2005. Cell type analysis of functional fetal dopamine cell suspension transplants in the striatum and substantia nigra of patients with Parkinson's disease. Brain 128, 1498–1510.

Moore, A.E., Cicchetti, F., Hennen, J., Isacson, O., 2001. Parkinsonian motor deficits are reflected by proportional A9/A10 dopamine neuron degeneration in the rat. Exp. Neurol. 172, 363–376.

Nelder, J.A., Wedderburn, R.W.M., 1972. Generalized Linear Models. J. R. Stat. Soc. A 135, 370–384.

Olsen, S.K., Li, J.Y., Bromleigh, C., Eliseenkova, A.V., Ibrahimi, O.A., Lao, Z., Zhang, F., Linhardt, R.J., Joyner, A.L., Mohammadi, M., 2006. Structural basis by which alternative splicing modulates the organizer activity of *FGF8* in the brain. Genes. Dev. 20, 185–198.

Omodei, D., Acampora, D., Mancuso, P., Prakash, N., Di Giovannantonio, L.G., Wurst, W., Simeone, A., 2008. Anterior-posterior graded response to Otx2 controls proliferation and differentiation of dopaminergic progenitors in the ventral mesencephalon. Development 135, 3459–3470.

Parent, A., 1996. Carpenter's Human Neuroanatomy. Williams & Wilkins, Baltimore.

Paxinos, G., 2004. The Rat Nervous. in: System, G. (Ed.), Paxinos. Elsevier, London.

Prakash, N., Brodski, C., Naserke, T., Puelles, E., Gogoi, R., Hall, A., Panhuysen, M., Echevarria, D., Sussel, L., et al., 2006. A *Wnt1*-regulated genetic network controls the identity and fate of midbrain-dopaminergic progenitors *in vivo*. Development 133, 89–98.

Prakash, N., Wurst, W., 2006. Genetic networks controlling the development of midbrain dopaminergic neurons. J. Physiol. 575, 403–410.

Puelles, E., Annino, A., Tuorto, F., Usiello, A., Acampora, D., Czerny, T., Brodski, C., Ang, S.L., Wurst, W., Simeone, A., 2004. Otx2 regulates the extent, identity and fate of neuronal progenitor domains in the ventral midbrain. Development 131, 2037–2048.

Saarimaki-Vire, J., Peltopuro, P., Lahti, L., Naserke, T., Blak, A.A., Vogt Weisenhorn, D.M., Yu, K., Ornitz, D.M., Wurst, W., Partanen, J., 2007. Fibroblast growth factor receptors cooperate to regulate neural progenitor properties in the developing midbrain and hindbrain. J. Neurosci. 27, 8581–8592.

Sawamoto, K., Nakao, N., Kobayashi, K., Matsushita, N., Takahashi, H., Kakishita, K., Yamamoto, A., Yoshizaki, T., Terashima, T., et al., 2001. Visualization, direct isolation, and transplantation of midbrain dopaminergic neurons. Proc. Natl. Acad. Sci. USA 98, 6423–6428.

Sgaier, S.K., Lao, Z., Villanueva, M.P., Berenshteyn, F., Stephen, D., Turnbull, R.K., Joyner, A.L., 2007. Genetic subdivision of the tectum and cerebellum into functionally related regions based on differential sensitivity to engrailed proteins. Development 134, 2325–2335.

Sidman, R.L., 1968. Development of interneuronal connections in brains of mutant mice. in: Carlson, F.D. (Ed.), In Physiological and Biochemical Aspects of Nervous Integration. Prentice-Hall, Inc., Englewood Cliffs.

Simon, H.H., Saueressig, H., Wurst, W., Goulding, M.D., O'Leary, D.D., 2001. Fate of midbrain dopaminergic neurons controlled by the engrailed genes. J. Neurosci. 21, 3126–3134.

Simon, H.H., Thuret, S., Alberi, L., 2004. Midbrain dopaminergic neurons: control of their cell fate by the engrailed transcription factors. Cell. Tissue. Res. 318, 53–61.

Thomas, K.R., Musci, T.S., Neumann, P.E., Capecchi, M.R., 1991. Swaying is a mutant allele of the proto-oncogene Wnt-1. Cell 67, 969–976.

Thompson, L., Barraud, P., Andersson, E., Kirik, D., Bjorklund, A., 2005. Identification of dopaminergic neurons of nigral and ventral tegmental area subtypes in grafts of fetal ventral mesencephalon based on cell morphology, protein expression, and efferent projections. J. Neurosci. 25, 6467–6477.

Uhl, G.R., Hedreen, J.C., Price, D.L., 1985. Parkinson's disease: loss of neurons from the ventral tegmental area contralateral to therapeutic surgical lesions. Neurology 35, 1215–1218.

Woolf, N.J., 1991. Cholinergic systems in mammalian brain and spinal cord. Prog. Neurobiol. 37, 475–524.

White, H., 1980. A heteroskedasticity-consistent covariance matrix estimator and a direct test for heteroskedasticity. Econometrica 48, 817–838.

Wurst, W., Auerbach, A.B., Joyner, A.L., 1994. Multiple developmental defects in Engrailed-1 mutant mice: an early mid-hindbrain deletion and patterning defects in forelimbs and sternum. Development 120, 2065–2075.

Ye, W., Shimamura, K., Rubenstein, J.L., Hynes, M.A., Rosenthal, A., 1998. FGF and Shh signals control dopaminergic and serotonergic cell fate in the anterior neural plate. Cell 93, 755–766.

Zervas, M., Blaess, S., Joyner, A.L., 2005. Classical embryological studies and modern genetic analysis of midbrain and cerebellum development. Curr. Top. Dev. Biol. 69, 101–138.

Zervas, M., Millet, S., Ahn, S., Joyner, A.L., 2004. Cell behaviors and genetic lineages of the mesencephalon and rhombomere 1. Neuron 43, 345–357.